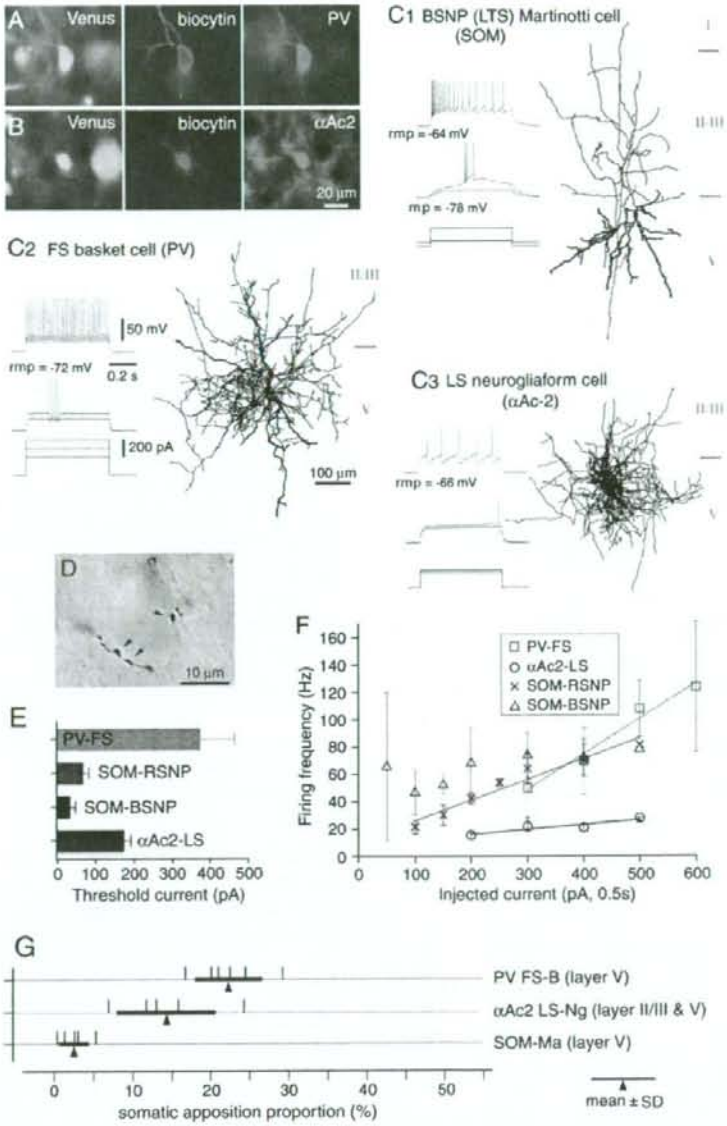

Figure 5. Correlation of physiological, chemical, and morphological characteristics in Venus-expressing cells. (*A*,*B*) Immunohistochemical identification of electrically recorded Venus cells labeled by biocytin as parvalbumin- (PV) or α-actinin-2- (αAc2) positive, respectively. (*C*) Firing patterns and morphologies of layer V Venus cells. Somata and dendrites are shown in black, and axons in red. (*C1*) a somatostatin (SOM)–positive BSNP Martinotti cell. LTS was induced from a hyperpolarized potential generated by d.c. somatic current injection (−37 pA). (*C2*) a parvalbumin-positive FS basket cell. (*C3*) an α-actinin-2–positive LS neurogliaform cell. (*D*) Bouton appositions of a Venus- and parvalbumin-positive FS basket cell onto another unstained soma (arrows). (*E*) Threshold currents necessary to induce spikes in response to depolarizing pulses. (*F*) Relationship between firing frequency and current strength. Firing frequency was calculated from the median of spike intervals in response to depolarizing current pulses with duration of 0.5 s. Solid lines indicate simple regression fits for parvalbumin-positive FS, α-actinin-2–positive LS, and somatostatin-positive RSNP cells. (*G*) Comparisons of the proportion of axonal boutons making appositions onto somata in the different nonpyramidal cell types in VGAT-Venus rats. Three subtypes were investigated: 6 parvalbumin-positive FS basket cells (layer V), 5 somatostatin-positive Martinotti cells (layer V), and 5 α-actinin-2–positive LS neurogliaform cells (3 in layer II/III and 2 in layer V). A comparison of these proportions of VGAT-Venus rats with those of wild-type rats is available in the Fig. 9. Abbreviations: mp, membrane potential; rmp, resting mp.

μm^2, $n = 21$; Fig. 7*B*), somewhat larger than those recorded in slices from wild-type rats (131 ± 34 μm^2, maximum = 202 μm^2, $n = 14$) (Kawaguchi et al. 2006), and included cells with similar size to layer V pyramidal cells in the same cortical regions (pyramidal cells projecting to the contralateral striatum, 224 ± 60 μm^2, maximum = 396 μm^2, $n = 19$; pyramidal cells projecting to the pons, 262 ± 45 μm^2, maximum = 360 μm^2, $n = 9$) (Morishima and Kawaguchi 2006). The use of VGAT-Venus rats

Table 4
Electrophysiological properties of nonpyramidal cell subtypes in frontal cortex of VGAT-Venus rats

Cell type	*N*	Resting potential (mV)	Input resistance (M)	Spike half-width (ms)	Threshold current[a] (pA)
PV-FS cells (layer V)	11	−71 ± 3	73 ± 15	0.41 ± 0.07	378 ± 88
SOM-RSNP cells (layer V)	7	−62 ± 3	170 ± 40	0.57 ± 0.04	71 ± 37
SOM-BSNP cells (layer V)	8	−60 ± 4	417 ± 138	0.6 ± 0.12	38 ± 33
αAc2-LS cells (layer II/III, V)	6[b]	−68 ± 2	126 ± 26	0.69 ± 0.06	178 ± 39
ANOVA/post hoc test		SOM > PV	SOM > PV	SOM > PV	PV > SOM
(Tukey test, $P < 0.05$)		SOM > αAc2	SOM-BSNP > SOM-RS	αAc2 > PV	PV > αAc2
			SOM-BSNP > αAc2		αAc2 > SOM

Note: Data are mean ± SD. *N*, number of cells. PV, parvalbumin; SOM, somatostatin; αAc2, α-actinin-2.
[a]Depolarizing current pulse of 0.5 s to induce spikes.
[b]4 in layer II/III and 2 in layer V.

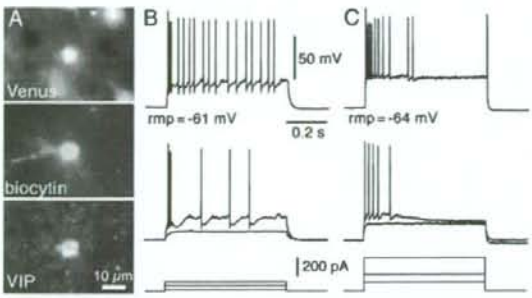

Figure 6. Venus-expressing VIP cells in layer II/III. (*A*) Immunohistochemical identification of recorded Venus-positive cells labeled by biocytin and showing VIP immunofluorescence. (*B*) A VIP cell showed the initial short-duration depolarizing hump with several spikes on it, followed by spike firing with irregular intervals. (*C*) Another VIP cell showed strong adaptation of spike firing in response to depolarizing current pulses and also irregular spike intervals.

allowed us to record nonpyramidal cells in an unbiased way irrespective of the soma size and shape.

Although the distribution of somatic size in FS cells was continuous from smaller to larger neurons (Fig. 7*B*), we looked for correlation between physiological properties and somatic size in 15 FS cells whose somata were stained with biocytin (maximum of the cross-sectional somatic area: 214 ± 65 μm^2; range, 128–311 μm^2). We did not find distinct differences in firing patterns between smaller and larger FS cells, but there was a weak correlation between input resistance and somatic size (c.c. = 0.32, $P = 0.25$; 103 ± 44 MΩ in 5 smaller cells and 69 ± 6 MΩ in 5 larger cells). The morphology of dendritic arborizations was investigated in FS basket cells whose dendrites and axons were sufficiently stained. The somatic size of FS cells correlated with the maximum vertical elongation of dendrites (c.c. = 0.55) (Fig. 7*A*), but not with the maximum horizontal distance (c.c. = 0.12) (Fig. 7*C*). Lager FS cells extended dendrites more widely in a vertical direction. Maximum vertical dendritic elongation was independent of somatic depth within layer V (c.c. = 0.06). This suggests that chemically and physiologically homogeneous FS cells are heterogeneous in their dendritic vertical dimensions, but have relatively uniform horizontal (columnar) dendritic dimensions (Fig. 7*C*). Findings were similar when observations were repeated in wild-type rats, as shown in the Appendix (Fig. 10). These data suggest that individual nonpyramidal cell subtypes, defined by combination of the spike firing, chemical expression, and axonal arborization patterns, show type-specific horizontal dendritic extensions.

Discussion

By applying BAC technology to rats, we generated, for the first time, transgenic rats with selective Venus fluorescence in GABAergic neurons. In certain brain areas, non-GABAergic neurons were labeled with Venus, but these areas were rarely overlapping in our 2 transgenic lines. Thus, at least one transgenic line can be used for selective identification of GABA cells in most areas of the forebrain. In the neocortex, we utilized the selective expression of Venus in GABAergic neurons to dissociate cortical interneurons into subtypes based on their chemical, physiological, and morphological characteristics. This is the first time that quantitative assessment of cortical interneurons using the above 6 chemical markers has been applied simultaneously to the full GABAergic cell population in the neocortex.

Selective Fluorescence Labeling of Forebrain GABA Cells in BAC Transgenic Rats

The biosynthetic enzyme for GABA, GAD, has 2 isoforms, GAD65 and GAD67. In transgenic mice produced using one of the 2 GAD promoters, only subpopulations of GABAergic cells are labeled with GFP (Oliva et al. 2000; Chattopadhyaya et al. 2004; Lopez-Bendito et al. 2004; Ma et al. 2006; Xu et al. 2006). In GAD67-GFP knock-in mice, most GABA cells are fluorescently labeled, but cells expressing only GAD65 may not be labeled. Furthermore, in GAD67-GFP knock-in mice, the GABA content is decreased because of the deletion of one GAD67 allele (Tamamaki et al. 2003). This reduction of GABA content may affect circuit formation, especially during development (Hensch 2005). Because the gene length of VGAT (~5 kb) is much shorter than those of GAD67 (~45 kb) and GAD65 (~80 kb) (Yanagawa et al. 1997; Makinae et al. 2000; Ebihara et al. 2003), we were able to construct a BAC clone containing the entire structure of VGAT, including regulatory sequences near the gene itself, to selectively label GABAergic neurons in rats. GABAergic neurons are widespread in the mammalian CNS, whereas glycinergic neurons are largely restricted to the spinal cord and brainstem (Esclapez et al. 1994; Legendre 2001). VGAT is the vesicular transporter not only for GABA but also for glycine (Sagne et al. 1997; Chaudhry et al. 1998). Therefore, it remains to be investigated whether both GABAergic and glycinergic cells are labeled with Venus in the spinal cord and brainstem.

We found Venus expression in non-GABAergic cells in a few regions, such as the relay nuclei of the thalamus in VGAT-Venus-A rats and the CA1 region of the hippocampus in VGAT-Venus-B rats. Even in these regions, however, the other line showed correct expression of Venus. Therefore, one of these 2 lines

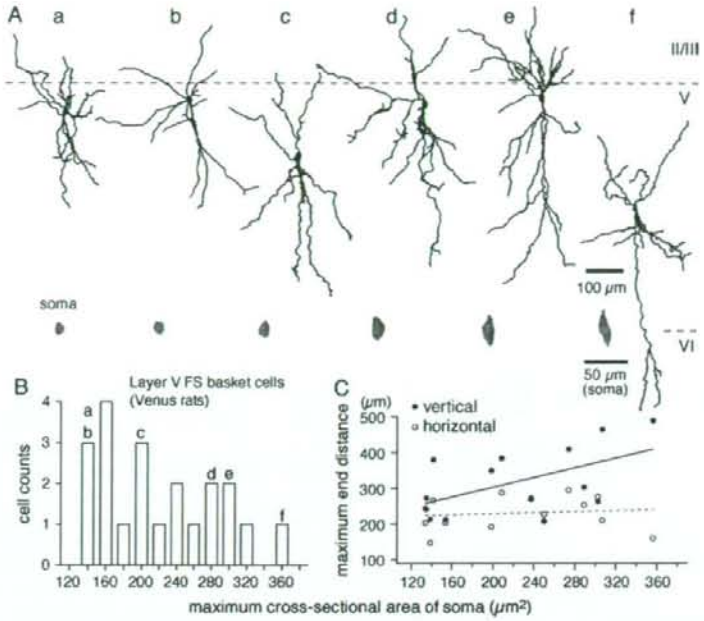

Figure 7. Large variability in the somatic size of layer V FS basket cells recorded from VGAT-Venus rats. (*A*) Dendritic reconstructions of 6 FS basket cells (a–f) in layer V sorted (left to right) according to increasing somatic cross-sectional area. Insets, somatic shapes. (*B*) Distribution of somatic cross-sectional areas. Each letter corresponds to the reconstructed cell shown in (*A*). (*C*) Relationship of dendritic arbors to the somatic cross-sectional areas. Horizontal and vertical maximum dendritic distances are calculated as the distances from somatic origin to the tip of the longest dendrite in horizontal and vertical directions, respectively. The vertical, but not horizontal, maximum distance was correlated with somatic size.

should be selected according to the investigated nucleus, region, or layer.

In the neocortex there were also subtle differences in Venus expression between the 2 lines. In VGAT-Venus-A rats, almost all GABAergic cells expressed Venus, but some layer VI pyramidal cells were weakly labeled in nonfrontal cortical areas. In VGAT-Venus-B rats, Venus fluorescence was not observed in layer VI pyramidal cells, and there was also failure to label all GABAergic cells. Nonfluorescent GABA cells in the B line belonged to subpopulations of VIP, CCK, calretinin, or α-actinin-2 expressing cells. Parvalbumin- and somatostatin-positive cells were always positive for Venus. The differential expression of Venus among GABAergic subtypes in the B line may reflect differences in the developmental origins of GABAergic neurons. Parvalbumin- and somatostatin-positive cells originate within the medial ganglionic eminence, whereas calretinin-positive cells derive from the caudal ganglionic eminence (Xu et al. 2004). The site of generation within the ganglionic eminence and its timing are critical for interneuron subtype differentiation (Butt et al. 2005). Aberrant Venus expression in some non-GABAergic cells, and the lack of Venus in specific subpopulations of GABAergic cells, may result from a positional effect, in which transcriptional regulation of the transgene is influenced by the chromosomal sequences flanking the point of transgene integration (Bessis et al. 1995).

Cortical GABA Cell Type Organization

Most GABAergic cell types identified so far can be classified based on their differential expression of a few calcium-binding proteins and neuropeptides, although individual expression patterns often include multiple morphological subtypes. LS neurogliaform cells, however, have not yet been chemically characterized. In the hippocampus, the actin-binding protein, α-actinin-2, is expressed not only in the dendrites of pyramidal cells, but also in the somata of some interneurons (Wyszynski et al. 1998; Ratzliff and Soltesz 2001), including neurogliaform cells (Price et al. 2005). Using VGAT-Venus-A rats, we found that α-actinin-2 is expressed in a subpopulation of GABAergic cells of the frontal cortex that includes LS neurogliaform cells in both layers II/III and V. α-Actinin-2 LS neurogliaform cells had an intermediate current threshold for spike induction that fell between the values for parvalbumin-expressing FS and somatostatin-positive cells. The slope of firing frequency against the injected current was less sharp in α-actinin-2 LS neurogliaform cells than in parvalbumin and somatostatin cells, and LS cells fired action potentials at relatively constant intervals, similar to FS cells, but at a much lower frequency. GABAergic nonpyramidal cells could generally be divided into basket and nonbasket cells based on their innervation preference for somatic domains. Innervation patterns of α-actinin-2–expressing LS neurogliaform cells, however, were more variable in their tendency to choose somatic targets (Figs 5*G* and 9). These physiological, chemical, and morphological characteristics suggest that cortical neurogliaform cells are a functionally distinct subgroup of cortical GABAergic cells (Tamás et al. 2003; Price et al. 2005).

The functional diversity of cortical GABAergic interneurons in the cortex remains to be investigated (Nelson 2002; Yuste 2005). Because several chemical markers are differentially

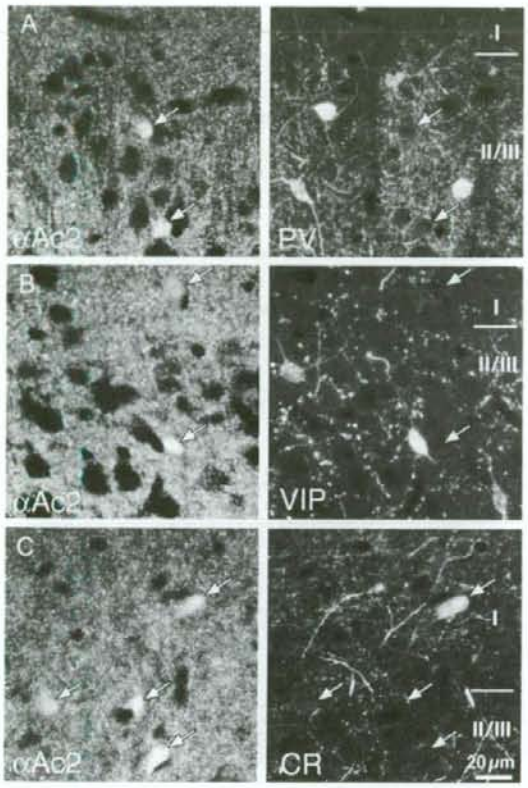

Figure 8. In the cortex, α-actinin-2–positive (αAc2) cells were separate from parvalbumin (PV) and VIP populations, but partially overlapped with calretinin cells. (*A*) Dual photomicrographs from the same microscopic field, showing the relationship of α-actinin-2- and parvalbumin-positive cells in wild-type rats. (*B*) Relationship of α-actinin-2 and VIP cells. (*C*) Relationship of α-actinin-2 and calretinin cells. Some α-actinin-2-positive cells showed calretinin immunofluorescence. Roman numerals correspond to cortical layers.

expressed in the somata of cortical GABAergic cells in a manner dependent on their developmental origin (Butt et al. 2005), it is important to know the proportion of all GABAergic neurons that can be identified from these markers. Our data demonstrate that α-actinin-2 is a chemical marker for neocortical LS neurogliaform cells, as has previously been shown for LS cells in the hippocampus (Price et al. 2005), and therefore allow the use of colocalization of 6 distinct chemical markers with Venus to estimate the proportion of GABA cells expressing at least one chemical marker (parvalbumin, somatostatin, CCK, VIP, calretinin, and α-actinin-2). We found that these 6 chemical markers cover the vast majority of GABAergic cells. Basket cells have been classified into several subtypes based on their differential expression of parvalbumin, VIP, CCK, or calretinin. Parvalbumin and CCK immunoreactivities are expressed in GABAergic cells with larger somata. Large CCK basket cells have been previously investigated in layer II/III where they are identifiable by their larger size relative to layer II/III pyramidal cells (Kawaguchi and Kubota 1998). Parvalbumin cells tend to be larger in deeper layers (Kubota et al. 1994), where they can sometimes be mistaken for layer V/VI pyramidal cells. In VGAT-Venus rats we

Table 5
Expression of the other chemical markers in α-actinin-2 cells of frontal cortex

Layer	PV	SOM	CR	VIP	CCK	CB
I	0% (75)	0% (74)	14.8% (81)	1.4% (74)	0% (78)	0% (33)
II/III	0% (81)	0% (101)	3.0% (101)	1.2% (82)	0% (97)	0% (48)
V	0% (17)	0% (20)	18.8% (16)	0% (19)	0% (14)	0% (12)
VI	0% (41)	0% (49)	16.2% (37)	0% (53)	2.4% (42)	0% (34)
Total	0% (214)	0% (244)	10.2% (235)	0.9% (228)	0.4% (231)	0% (127)

Note: Cells positive for a chemical marker/α-actinin-2 cells. PV, parvalbumin; SOM, somatostatin; CR, calretinin; CB, calbindin. Data are combined from 3 animals. ( ), number of cells positive for α-actinin-2 (denominator).

found large FS basket cells that were of similar size or shape to pyramidal cells, as well as much smaller neurons, and their vertical dendritic extent varied with somatic size. These data indicate basket cells having similar chemical and physiological characteristics can be further differentiated based on dendritic domains, even within the same layer. Because of the robust Venus fluorescence in our VGAT-Venus animals, we can now identify and record from neocortical nonpyramidal cells in an unbiased manner, irrespective of somatic size or shape.

Utility of VGAT-Venus Transgenic Rats

Largely as a result of technical advances such as gene targeting (knockout and knock-in) technology in ES cells, the mouse will continue to be a convenient mammalian model, especially for genetic and developmental studies. In contrast, the rat has for many years provided the most appropriate physiological and neurobiological model. The rat is useful for a whole range of physiological, surgical, and neurobiological manipulations that would be much more difficult in the mouse because of its smaller size (Phang 1993). Examples of such manipulations include the measurement of blood pressure, multiple automated blood sampling, and the introduction of probes into specific areas of the brain for electrophysiological recordings, cellular ablation, and drug delivery. In addition, the rat has been the preferred model for behavioral studies because rats are superior to mice in learning and generally less aggressive during handling. Furthermore, it should be possible to record Venus-positive cortical cells by direct visual guidance of 2-photon microscopy (Margrie et al. 2003). Given that cortical GABAergic neurons play a central role in generating appropriate behavioral output (Fuchs et al. 2007), VGAT-Venus rats will be an important tool for in vivo recording from cortical GABAergic neurons together with single cell fluorescence imaging.

In conclusion, the BAC technology described here permits specific fluorescent labeling of GABAergic neurons in the intact brain. This suggests possible genetic manipulation of GABAergic interneurons in the rat by driving Cre recombinase expression using the VGAT BAC construct. We expect VGAT-Venus transgenic rats to be highly useful for a multitude of in vitro or in vivo investigations of the structure and function of GABAergic neurons, both in basic research and in clinically oriented studies.

Appendix

We also investigated the following 3 characteristics in nonpyramidal cells of wild-type Wistar rats: 1) the colocalization pattern of α-actinin-2 with the other chemical markers at the somata to calculate the proportion of GABAergic cells expressing the chemical markers in VGAT-Venus rats; 2) the proportion of boutons from the nonpyramidal cells making somatic appositions in order to confirm the similarity of the somatic innervation patterns between the VGAT-Venus and wild-type

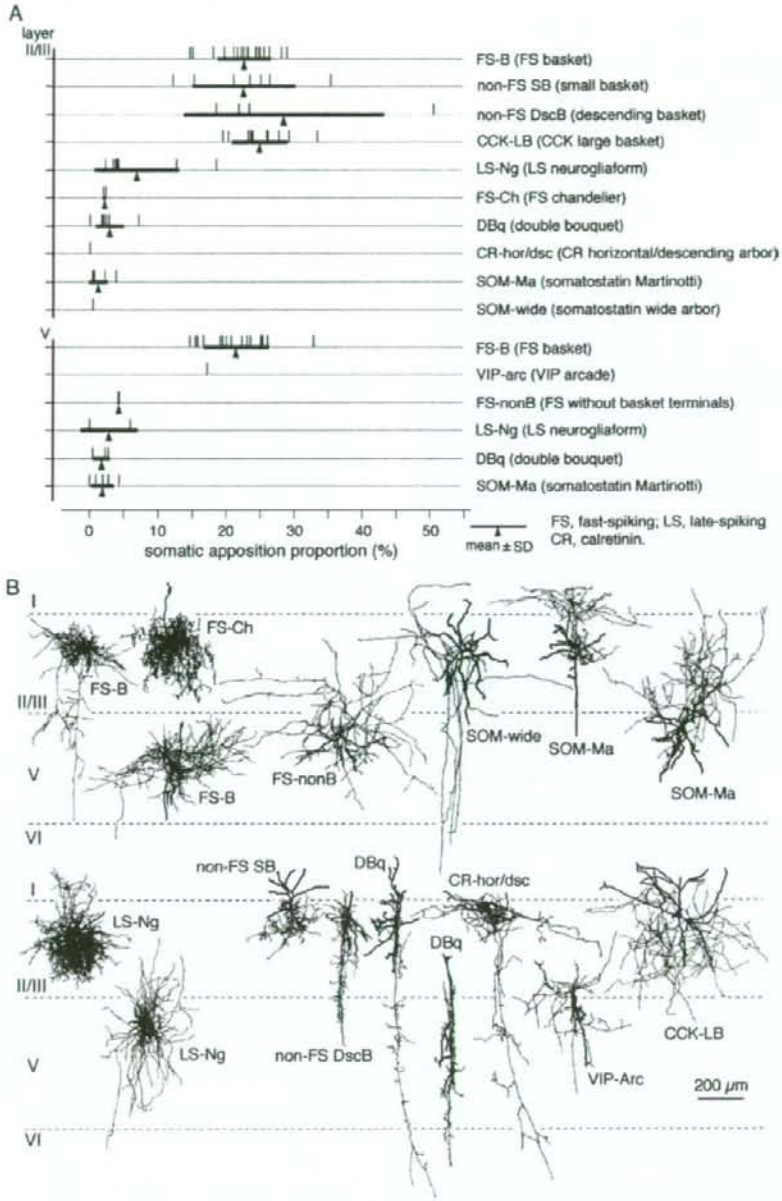

Figure 9. Somatic innervation patterns in wild-type rats. (*A*) Comparisons of the proportion of axonal boutons making appositions on other somata between nonpyramidal cell subtypes in wild-type rats. Basket and nonbasket classes were mostly differentiated. (*B*) Reconstructions of nonpyramidal cell subtypes. Somata and dendrites are shown in black, and axons in red. Ten subtypes were investigated in layer II/III: 18 FS basket cells, 2 FS chandelier cells, 7 LS neurogliaform cells, 6 somatostatin Martinotti cells, a somatostatin wide arbor cell, 11 CCK large basket cells, 7 small basket cells positive for VIP, CCK, or CRF, 4 descending basket cells positive for VIP or CRF, 7 double bouquet cells positive for VIP, CRF, or calretinin, and 1 calretinin horizontal/descending arbor cell. In layer V, 6 subtypes were investigated: 16 FS basket cells, 2 FS cells without basket terminals, 2 LS neurogliaform cells, 5 somatostatin Martinotti cells, 3 double bouquet cells positive for VIP, and a VIP arcade cell.

rats; and 3) the horizontal spread of dendrites, which, from the data of FS basket cells obtained from the VGAT-Venus rat appeared specific for each subtype.

To determine the frequency for colocalization of α-actinin-2 with the other chemical markers, we investigated the relationship of their immunofluorescences in the frontal cortex (Fig. 8). Parvalbumin-positive and somatostatin-positive cells did not express α-actinin-2, and only a very few VIP-positive and CCK-positive neurons were positive for α-actinin-2 (Table 5). However, some α-actinin-2-positive cells showed calretinin immunoreactivity, especially in layer I (14.8%),

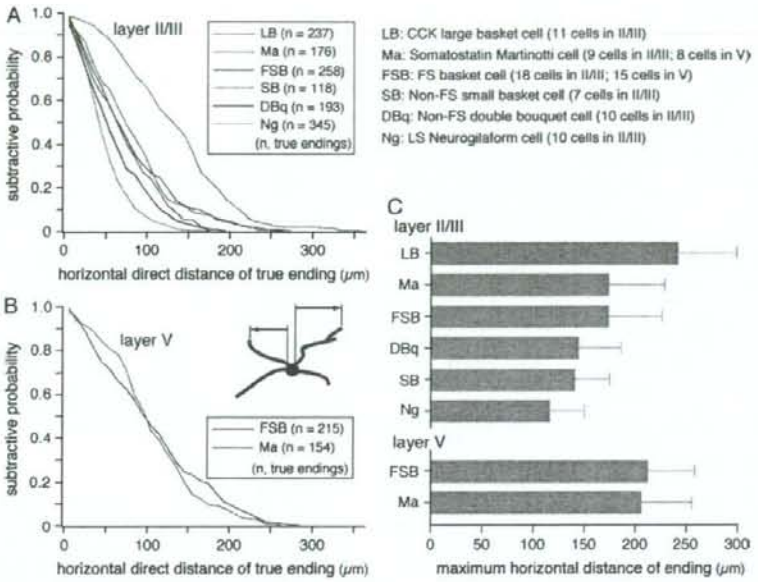

Figure 10. Dendritic horizontal extension of nonpyramidal cell subtypes. (*A*, *B*) Distributions of horizontal direct distances of true endings, measured from their somatic origins, in layers II/III and V, respectively. In layer II/III CCK large basket cells were wider than the other types ($P < 0.01$). The LS neurogliaform cells were narrower than the other types ($P < 0.01$). Double bouquet cells were narrower than CCK large basket, somatostatin Martinotti, and FS basket cells ($P < 0.01$). (*C*) Maximum horizontal dendritic spread of individual nonpyramidal cells. In layer II/III, CCK large basket cells had larger maximum dendritic spreads than did LS neurogliaform, non-FS small basket, double bouquet, and FS basket cells ($P < 0.01$), and somatostatin Martinotti cells ($P < 0.05$). FS basket cells had larger dendritic spreads than LS neurogliaform cells ($P < 0.05$).

layer V (18.8%), and layer VI (16.2%) (Table 5). Another calcium-binding protein, calbindin was not found in α-actinin-2 cells.

We compared the proportion of boutons apposed with target somata for 12 subtypes of nonpyramidal cells in wild-type rats, including previously recorded and stained cells by Karube et al. (2004), and also newly reconstructed cells (Fig. 9; 64 cells of 10 subtypes in layer II/III and 29 cells of 6 subtypes in layer V). These measurements suggest that, whereas nonpyramidal cell subtypes are different in their preferences for axonal innervation of somata, more than half of GABAergic boutons contact domains other than somata, even in basket cells. The somatic apposition proportions of LS neurogliaform cells were found to be more variable in wild-type rats.

We compared the horizontal spread of dendrites among the 6 GABAergic cell subtypes previously described by Kawaguchi et al. (2006) (Fig. 10). The mean horizontal length of dendrites (as measured from soma to uncut endings) of the layer V FS basket cell was 117 ± 68 μm (249 true endings from 14 cells) in Venus rats, and 109 ± 66 μm (215 from 15 cells) in tissue from wild-type rats (Fig. 10*B*). Horizontal dendritic distances of layer V somatostatin Martinotti cells were similar, being 109 ± 55 μm (154 from 8 cells). In layer II/III, dendrites of CCK large basket cells had a longer horizontal reach than dendrites in LS neurogliaform, double bouquet, non-FS small basket, FS basket, and somatostatin Martinotti cells ($P < 0.01$; Fig. 10*A*). LS neurogliaform cells were also narrower than all other types ($P < 0.01$), and double bouquet cells were narrower than the CCK large basket, somatostatin Martinotti, and FS basket cells ($P < 0.01$). Next, the maximum horizontal distance (horizontal spread) was obtained from individual cells. The maximum horizontal dendritic spread in layer V FS basket cells was 230 ± 47 μm (14 cells) from Venus rats and 212 ± 47 μm (15 cells) from wild-type rats (Fig. 10*C*). That of layer V somatostatin Martinotti cells was similar (206 ± 50 μm, 8 cells). In layer II/III, CCK large basket cells had larger maximum horizontal spread than LS neurogliaform, non-FS small basket, double bouquet, and FS basket cells ($P < 0.01$; Fig. 10*C*).

These observations from wild-type rats, combined with those from VGAT-Venus rats, support the normal differentiation of cortical GABAergic cells in VGAT-Venus rats, and demonstrate that α-actinin-2 is a useful chemical marker for a distinct cortical interneuron subtype. Further, they suggest a cortical interneurons maintain an inherent, cell type-specific horizontal dendritic territory.

Notes

The authors thank Ms M. Saito and Mr Y. Ito for technical assistances, and Drs A. Gulledge, Y. Kubota and M. Morishima for discussion and comments. We also thank staffs in Center for Experimental Animals, National Institute for Physiological Sciences (NIPS). We are grateful to Dr A. Miyawaki for providing pCS2-Venus, to Dr M. D. Lalioti for pKOV-Kan and pDF25 plasmids, to Dr A.H. Beggs for an antiserum against α-actinin-2, and to Dr N. Tamamaki for a rabbit antiserum against eGFP. We are also grateful to Dr T. Kosaka for helpful discussions about Venus expression patterns. This work was supported by Grant-in-Aids for Scientific Research from the Ministry of Education, Culture, Sports, Science and Technology (MEXT) and on Psychiatric and Neurological Diseases and Mental Health from the Ministry of Health, Labor and Welfare of Japan, and also supported by The Uehara Memorial Foundation and Brain Science Foundation. This paper is dedicated to the late Ms Kazuko Kawaguchi who had supported Y.K. continuously.
Conflict of Interest: None declared.

Address correspondence to Yasuo Kawaguchi, Division of Cerebral Circuitry, National Institute for Physiological Sciences, Myodaiji, Okazaki 444-8585, Japan. Email: yasuo@nips.ac.jp, or to Yuchio Yanagawa, Department of Genetic and Behavioral Neuroscience, Gunma University Graduate School of Medicine, Maebashi 371-8511, Japan. Email: yanagawa@med.gunma-u.ac.jp.

References

Bessis A, Salmon AM, Zoli M, Le Novere N, Picciotto M, Changeux JP. 1995. Promoter elements conferring neuron-specific expression of the beta 2-subunit of the neuronal nicotinic acetylcholine receptor studied in vitro and in transgenic mice. Neuroscience. 69: 807–819.

Butt SJ, Fuccillo M, Nery S, Noctor S, Kriegstein A, Corbin JG, Fishell G. 2005. The temporal and spatial origins of cortical interneurons predict their physiological subtype. Neuron. 48:591–604.
Cauli B, Porter JT, Tsuzuki K, Lambolez B, Rossier J, Quenet B, Audinat E. 2000. Classification of fusiform neocortical interneurons based on unsupervised clustering. Proc Natl Acad Sci USA. 97:6144–6149.
Chattopadhyaya B, Di Cristo G, Higashiyama H, Knott GW, Kuhlman SJ, Welker E, Huang ZJ. 2004. Experience and activity-dependent maturation of perisomatic GABAergic innervation in primary visual cortex during a postnatal critical period. J Neurosci. 24: 9598–9611.
Chaudhry FA, Reimer RJ, Bellocchio EE, Danbolt NC, Osen KK, Edwards RH, Storm-Mathisen J. 1998. The vesicular GABA transporter, VGAT, localizes to synaptic vesicles in sets of glycinergic as well as GABAergic neurons. J Neurosci. 18:9733–9750.
DeFelipe J, Hendry SH, Jones EG. 1986. A correlative electron microscopic study of basket cells and large GABAergic neurons in the monkey sensory-motor cortex. Neuroscience. 17:991–1009.
Ebihara S, Obata K, Yanagawa Y. 2003. Mouse vesicular GABA transporter gene: genomic organization, transcriptional regulation and chromosomal localization. Brain Res Mol Brain Res. 110:126–139.
Esclapez M, Tillakaratne NJ, Kaufman DL, Tobin AJ, Houser CR. 1994. Comparative localization of 2 forms of glutamic acid decarboxylase and their mRNAs in rat brain supports the concept of functional differences between the forms. J Neurosci. 14:1834–1855.
Ferezou I, Cauli B, Hill EL, Rossier J, Hamel E, Lambolez B. 2002. 5-HT_3 receptors mediate serotonergic fast synaptic excitation of neocortical vasoactive intestinal peptide/cholecystokinin interneurons. J Neurosci. 22:7389–7397.
Fuchs EC, Zivkovic AR, Cunningham MO, Middleton S, LeBeau FEN, Bannerman DM, Rozov A, Whittington MA, Traub RD, Rawlins JNP, et al. 2007. Recruitment of parvalbumin-positive interneurons determines hippocampal function and associated behavior. Neuron. 53:591–604.
Gonchar Y, Burkhalter A. 1997. Three distinct families of GABAergic neurons in rat visual cortex. Cereb Cortex. 7:347–358.
Gulledge AT, Park SB, Kawaguchi Y, Stuart GJ. 2007. Heterogeneity of phasic cholinergic signalling in neocortical neurons. J Neurophysiol. 97:2215–2229.
Gupta A, Wang Y, Markram H. 2000. Organizing principles for a diversity of GABAergic interneurons and synapses in the neocortex. Science. 287:273–278.
Heintz N. 2001. BAC to the future: the use of BAC transgenic mice for neuroscience research. Nat Rev Neurosci. 2: 861–870.
Hensch TK. 2005. Critical period plasticity in local cortical circuits. Nat Rev Neurosci 6:877–888.
Jones EG. 1975. Varieties and distribution of non-pyramidal cells in the somatic sensory cortex of the squirrel monkey. J Comp Neurol. 160:205–267.
Karube F, Kubota Y, Kawaguchi Y. 2004. Axon branching and synaptic bouton phenotypes in GABAergic nonpyramidal cell subtypes. J Neurosci. 24:2853–2865.
Kawaguchi Y. 1997. Selective cholinergic modulation of cortical GABAergic cell subtypes. J Neurophysiol. 78:1743–1747.
Kawaguchi Y, Karube F, Kubota Y. 2006. Dendritic branch typing and spine expression patterns in cortical nonpyramidal cells. Cereb Cortex. 16:696–711.
Kawaguchi Y, Kondo S. 2002. Parvalbumin, somatostatin and cholecystokinin as chemical markers for specific GABAergic interneuron types in the rat frontal cortex. J Neurocytol. 31:277–287.
Kawaguchi Y, Kubota Y. 1993. Correlation of physiological subgroupings of nonpyramidal cells with parvalbumin- and calbindin$_{D28k}$-immunoreactive neurons in layer V of rat frontal cortex. J Neurophysiol. 70:387–396.
Kawaguchi Y, Kubota Y. 1996. Physiological and morphological identification of somatostatin- or vasoactive intestinal polypeptide-containing cells among GABAergic cell subtypes in rat frontal cortex. J Neurosci. 16:2701–2715.
Kawaguchi Y, Kubota Y. 1997. GABAergic cell subtypes and their synaptic connections in rat frontal cortex. Cereb Cortex. 7: 476–486.
Kawaguchi Y, Kubota Y. 1998. Neurochemical features and synaptic connections of large physiologically-identified GABAergic cells in the rat frontal cortex. Neuroscience. 85:677–701.
Kubota Y, Hatada S, Kondo S, Karube F, Kawaguchi Y. 2007. Neocortical inhibitory terminals innervate dendritic spines targeted by thalamocortical afferents. J Neurosci. 27:1139–1150.
Kubota Y, Hattori R, Yui Y. 1994. Three distinct subpopulations of GABAergic neurons in rat frontal agranular cortex. Brain Res. 649:159–173.
Kubota Y, Kawaguchi Y. 1997. Two distinct subgroups of cholecystokinin-immunoreactive cortical interneurons. Brain Res. 752:175–183.
Lalioti M, Heath J. 2001. A new method for generating point mutations in bacterial artificial chromosomes by homologous recombination in Escherichia coli. Nucleic Acids Res. 29:E14.
Legendre P. 2001. The glycinergic inhibitory synapse. Cell Mol Life Sci. 58:760–793.
Lopez-Bendito G, Sturgess K, Erdelyi F, Szabo G, Molnar Z, Paulsen O. 2004. Preferential origin and layer destination of GAD65-GFP cortical interneurons. Cereb Cortex. 14:1122–1133.
Ma Y, Hu H, Berrebi AS, Mathers PH, Agmon A. 2006. Distinct subtypes of somatostatin-containing neocortical interneurons revealed in transgenic mice. J Neurosci. 26:5069–5082.
Makinae K, Kobayashi T, Kobayashi T, Shinkawa H, Sakagami H, Kondo H, Tashiro F, Miyazaki J, Obata K, Tamura S, et al. 2000. Structure of the mouse glutamate decarboxylase 65 gene and its promoter: preferential expression of its promoter in the GABAergic neurons of transgenic mice. J Neurochem. 75:1429–1437.
Margrie TW, Meyer AH, Caputi A, Monyer H, Hasan MT, Schaefer AT, Denk W, Brecht M. 2003. Targeted whole-cell recordings in the mammalian brain in vivo. Neuron. 39:911–918.
Marin-Padilla M. 1969. Origin of the pericellular baskets of the pyramidal cells of the human motor cortex: a Golgi study. Brain Res. 14:633–646.
Markram H, Toledo-Rodriguez M, Wang Y, Gupta A, Silberberg G, Wu C. 2004. Interneurons of the neocortical inhibitory system. Nat Rev Neurosci. 5:793–807.
Melchitzky DS, Eggan SM, Lewis DA. 2005. Synaptic targets of calretinin-containing axon terminals in macaque monkey prefrontal cortex. Neuroscience. 130:185–195.
Meyer AH, Katona I, Blatow M, Rozov A, Monyer H. 2002. In vivo labeling of parvalbumin-positive interneurons and analysis of electrical coupling in identified neurons. J Neurosci. 22:7055–7064.
Morishima M, Kawaguchi Y. 2006. Recurrent connection patterns of corticostriatal pyramidal cells in frontal cortex. J Neurosci. 26:4394–4405.
Nagai T, Ibata K, Park ES, Kubota M, Mikoshiba K, Miyawaki A. 2002. A variant of yellow fluorescent protein with fast and efficient maturation for cell-biological applications. Nat Biotechnol. 20: 87–90.
Nelson S. 2002. Cortical microcircuits: diverse or canonical? Neuron. 36:19–27.
Oliva AA, Jr., Jiang M, Lam T, Smith KL, Swann JW. 2000. Novel hippocampal interneuronal subtypes identified using transgenic mice that express green fluorescent protein in GABAergic interneurons. J Neurosci. 20:3354–3368.
Phang C-H. 1993. Introduction to the physiology and husbandry of the rat. In: Murphy D, Carter DA, editors. Methods in molecular biology: transgenesis techniques. Totowa, NJ: Humana Press. p. 247–251.
Porter JT, Cauli B, Tsuzuki K, Lambolez B, Rossier J, Audinat E. 1999. Selective excitation of subtypes of neocortical interneurons by nicotinic receptors. J Neurosci. 19:5228–5235.
Price CJ, Cauli B, Kovacs ER, Kulik A, Lambolez B, Shigemoto R, Capogna M. 2005. Neurogliaform neurons form a novel inhibitory network in the hippocampal CA1 area. J Neurosci. 25:6775–6786.
Ratzliff AD, Soltesz I. 2001. Differential immunoreactivity for alpha-actinin-2, an N-methyl-D-aspartate-receptor/actin binding protein, in hippocampal interneurons. Neuroscience. 103:337–349.
Sagne C, El Mestikawy S, Isambert MF, Hamon M, Henry JP, Giros B, Gasnier B. 1997. Cloning of a functional vesicular GABA and glycine transporter by screening of genome databases. FEBS Lett. 417:177–183.

Somogyi P, Klausberger T. 2005. Defined types of cortical interneurone structure space and spike timing in the hippocampus. J Physiol. 562:9–26.
Somogyi P, Tamás G, Lujan R, Buhl EH. 1998. Salient features of synaptic organisation in the cerebral cortex. Brain Res Brain Res Rev. 26:113–135.
Sugino K, Hempel CM, Miller MN, Hattox AM, Shapiro P, Wu C, Huang ZJ, Nelson SB. 2006. Molecular taxonomy of major neuronal classes in the adult mouse forebrain. Nat Neurosci. 9:99–107.
Takahashi R, Hirabayashi M, Ueda M. 1999. Production of transgenic rats using cryopreserved pronuclear-stage zygotes. Transgenic Res. 8:397–400.
Tamamaki N, Yanagawa Y, Tomioka R, Miyazaki J, Obata K, Kaneko T. 2003. Green fluorescent protein expression and colocalization with calretinin, parvalbumin, and somatostatin in the GAD67-GFP knock-in mouse. J Comp Neurol. 467:60–79.
Tamás G, Lörincz A, Simon A, Szabadics J. 2003. Identified sources and targets of slow inhibition in the neocortex. Science. 299: 1902–1905.
Toledo-Rodriguez M, Blumenfeld B, Wu C, Luo J, Attali B, Goodman P, Markram H. 2004. Correlation maps allow neuronal electrical properties to be predicted from single-cell gene expression profiles in rat neocortex. Cereb Cortex. 14:1310–1327.
Wang Y, Gupta A, Toledo-Rodriguez M, Wu CZ, Markram H. 2002. Anatomical, physiological, molecular and circuit properties of nest basket cells in the developing somatosensory cortex. Cereb Cortex. 12:395–410.
Wyszynski M, Kharazia V, Shanghvi R, Rao A, Beggs AH, Craig AM, Weinberg R, Sheng M. 1998. Differential regional expression and ultrastructural localization of alpha-actinin-2, a putative NMDA receptor-anchoring protein, in rat brain. J Neurosci. 18:1383–1392.
Xu Q, Cobos I, De La Cruz E, Rubenstein JL, Anderson SA. 2004. Origins of cortical interneuron subtypes. J Neurosci. 24:2612–2622
Xu X, Roby KD, Callaway EM. 2006. Mouse cortical inhibitory neuron type that coexpresses somatostatin and calretinin. J Comp Neurol. 499:144–160.
Yanagawa Y, Kobayashi T, Kamei T, Ishii K, Nishijima M, Takaku A, Tamura S. 1997. Structure and alternative promoters of the mouse glutamic acid decarboxylase 67 gene. Biochem J. 326:573–578.
Yuste R. 2005. Origin and classification of neocortical interneurons. Neuron. 48:524–527.

Cellular/Molecular

Firing-Pattern-Dependent Specificity of Cortical Excitatory Feed-Forward Subnetworks

Takeshi Otsuka and Yasuo Kawaguchi
Division of Cerebral Circuitry, National Institute for Physiological Sciences, Okazaki, Aichi 444-8787, Japan

The cortical circuit includes networks of highly interconnected pyramidal neurons. Here, we investigated whether pyramidal cells form subnetworks depending on pyramidal subtypes. We classified layer V (L5) pyramidal cells in rat frontal cortex into three physiological subtypes based on the presence (SA-d type) or absence (SA type) of an initial burst in neurons displaying slowly adapting spike trains, or fast spike frequency adaptation (FA type) against current pulse injections. Pyramidal cells projecting to the particular subcortical areas were correlated with the physiological subtypes. Focal glutamate stimulation of a L2/3 pyramidal cell induced EPSCs in SA and SA-d cells more frequently than in FA cells. FA cells in upper L5 received more inputs from the upper L2/3, and those in lower L5 received inputs from cells in lower L2/3, suggesting topographic interlaminar projections to FA cells. Dual recordings from L5 pyramidal cells revealed that common input probability that two L5 cells share inputs from a L2/3 cell was high in cell pairs of the same subtypes, compared with those in different subtype pairs. Furthermore, the common input probability was highly selective when cell pairs of the same subtypes, but not different subtypes, had connections between them. Our results suggest that L2/3 pyramidal cells selectively innervate L5 cells, depending on their firing subtypes.

Key words: **cortex; pyramidal cell; firing pattern; extracortical projection; connection specificity; interlaminar connection**

Introduction

The neocortex is a layered structure, and contains numerous types of excitatory and inhibitory neurons (DeFelipe and Fariñas, 1992; Kawaguchi and Kubota, 1997; Markram et al., 2004). Interlaminar excitatory connections are direction-selective, with the information originating in thalamic-receptive neurons transmitted first to excitatory neurons in superficial layers, and then relayed to deeper layers (Bureau et al., 2006; Lübke and Feldmeyer, 2007). As such a unit of cortical information processing, the cortex shows a columnar organization (Mountcastle, 1997). To facilitate the directional transfer of the information, pyramidal neurons selectively form synaptic connections. At finer scales within columns, the local circuitry can be divided into modules of selectively connected cells (Yoshimura et al., 2005). In layer V (L5) of the visual cortex, pairs of connected pyramidal cells are more likely to form connections to a third neuron than are unconnected pairs (Song et al., 2005). The divergent and convergent probabilities of interlaminar excitatory connections depend on the connectivity patterns of recipient and projecting cell pairs, respectively (Shepherd and Svoboda, 2005; Yoshimura et al., 2005; Kampa et al., 2006). These studies have been demonstrated that intralaminar and interlaminar connections of pyramidal cells are clustered into subnetworks.

Pyramidal cells, however, can be classified into several subtypes. Physiologically, cells firing burst of multiple spikes and regular spiking cells firing trains of single spikes during current pulse injection have been described (Connors et al., 1982; McCormick et al., 1985; Agmon and Connors, 1992; Cho et al., 2004). Pyramidal cells can be further classified based on the degree of the spike frequency adaptation during prolonged current injections (Gottlieb and Keller, 1997; Dégenètais et al., 2002; Chang and Luebke, 2007). Morphological analyses of dendritic branching patterns also revealed a diversity of pyramidal subtypes (Tsiola et al., 2003). In L5 pyramidal cells, a major source of subcortical projections, dendritic morphologies are correlated with their axonal projection targets and their firing patterns in some cortical areas (Chagnac-Amitai et al., 1990; Mason and Larkman, 1990; Hefti and Smith, 2000; Gao and Zheng, 2004; Morishima and Kawaguchi, 2006; Hattox and Nelson, 2007), suggesting that physiologically identified subtypes of L5 pyramidal cells sharing similar physiological characteristics represent functional output classes. Several studies have indicated that functional input-out connectivity of thalamocortical afferents and corticocortical connections differ between pyramidal subtypes (Agmon and Connors, 1992; Morishima and Kawaguchi, 2006; Schubert et al., 2006). However, it remains unknown whether these pyramidal subtypes form subnetworks.

Here, we investigated whether interlaminar connections from L2/3 to L5 pyramidal cells are segregated with regard to the subclass of L5 pyramidal cells. After quantitative identification of three firing subtypes among L5 pyramidal cells, we examined correlation of the firing subtypes with the subcortical projection

Received Sept. 8, 2008; accepted Sept. 20, 2008.

This work was supported by Grant-in-Aids for Scientific Research from the Ministry of Education, Culture, Sports, Science, and Technology (MEXT), Ministry of Health, Labor, and Welfare of Japan, the Uehara Memorial Foundation, and Brain Science Foundation to T.O. and Y.K. We thank A. Gulledge, T. Inoue, M. Morishima, M. Miyata, and Y. Kubota for helpful comments. We are grateful to M. Morishima for technical advice on the retrograde tracer experiment.

Correspondence should be addressed to Yasuo Kawaguchi, Division of Cerebral Circuitry, National Institute for Physiological Sciences, 5-1 Myodaiji-Higashiyama, Okazaki, Aichi 444-8787, Japan. E-mail: yasuo@nips.ac.jp.

DOI:10.1523/JNEUROSCI.1921-08.2008

 0270-6474/08/2811186-10$15.00/0

targets. We then investigated the spatial distribution of L2/3 cells innervating L5 pyramidal subtypes, and the divergence pattern from L2/3 to L5 cell pairs. Our results suggest that the interlaminar synaptic pathways originating from L2/3 are segregated according to L5 pyramidal subtypes, and that these subtype-dependent pathways are further segregated into modules of synaptically interconnected cells.

Materials and Methods

Whole-cell recordings in slice. All experiments were conducted in compliance with the guidelines for animal experimentation of the Okazaki National Research Institutes. Slices including frontal cortex were prepared from Wistar rats, aged postnatal day 19–23. Rats were anesthetized with isoflurane and decapitated; brains were removed, iced, and blocked for slicing. The blocked tissue was cut into 300 μm thick slices with a Microslicer (Dosaka EM), while being bathed in oxygenated Kreb's solution composed of (in mM): 126 NaCl, 2.5 KCl, 1.25 NaH_2PO_4, 1 $MgCl_2$, 2 $CaCl_2$, 26 $NaHCO_3$, and 10 glucose (310 ± 5 mOsm/L, pH 7.4; bubbled with 95%O_2 and 5%CO_2). The slices were incubated at room temperature for at least 1 h in oxygenated Kreb's solution containing 0.2 mM ascorbic acid and 4 mM lactic acid. The slice was transferred to a recording chamber mounted on an upright microscope (Carl Zeiss) and continuously perfused with oxygenated Kreb's solution. Temperature of the bath solution in the recording chamber was adjusted to 30°C. Whole-cell recordings were performed using an EPC-9 double amplifier (HEKA Elektronik) controlled with a Macintosh computer running Pulse software (HEKA Elektronik). Electrodes were pulled from glass capillary tubes (Narishige) and fire-polished. The recording pipettes were filled with a solution containing (in mM): 130 potassium methylsulfate, 0.5 EGTA, 2 $MgCl_2$, 2 Na_2ATP, 0.2 GTP, 20 HEPES, 0.1 leupeptin and 0.75% biocytin (pH 7.2, 290 ± 5 mOsm/L) and had resistances of 5–7 MΩ in the bath. In experiments using glutamate stimulation, 1 mM sodium glutamate were dissolved in Kreb's solution and filled into the same pipettes as the one for whole-cell recordings. To avoid cells with their axons cut a lot by slicing, we did not stimulate cells located at the surface of slices. Stimulated L2/3 cells were typically located 20–50 μm deep from the slice surface. We positioned the pipette filled with glutamate within 10 μm distance from the soma aimed to trigger the spike and added air pressure (5–10 psi, 50 ms duration) to eject the glutamate solution onto the target cell. To calculate the connection and common input probabilities using glutamate stimulation, we discarded L5 pyramidal cells without any EPSC induction and L5 pairs without any simultaneous EPSC induction, respectively. This means that the probabilities used did not include zero. Even if we included cases with no common inputs, but EPSCs in both L5 cells, we obtained similar results (supplemental Fig. 1, available at www.jneurosci.org as supplemental material). For the analysis of firing patterns of cells, recordings were obtained immediately (3 min maximum) after membrane rupture. To quantify the voltage sag in response to negative current pulse injections, we measured the voltage difference between the negative peak and the end of membrane potentials to the current pulse (amplitude, −500pA; duration, 1 s) applied from resting membrane potentials adjusted to −60 mV by DC current injections. Data are represented as mean ± SD and statistical difference between samples was tested using ANOVA. Significance was accepted when $p < 0.05$.

Retrograde labeling. To identify pyramidal subtypes, retrograde fluorescent tracer, Alexa Fluor 555-conjugated cholera toxin subunit B (Invitrogen) or rhodamine-labeled latex microspheres (Lumafluor), was injected into contralateral striatum, ipsilateral pontine nuclei, or contralateral frontal cortex using similar procedures described previously (Morishima and Kawaguchi, 2006). Animals were anesthetized with ketamine (40 mg/kg, i.m.) and xylazine (4 mg/kg, i.m.). After injection of fluorescent retrograde tracer, animals were fed for 2–3 d as a recovery period before slice experiments.

Histology. Slices containing cells intracellularly labeled with biocytin were fixed with a solution containing 4% paraformaldehyde, 1.25% glutaraldehyde, and 0.2% picric acid in PB. After rinsing in PB, slices were treated with PB containing 1% H_2O_2 for 20 min and were resectioned at a thickness of 50 μm. Sections were then incubated with avidin-biotin-horseradish peroxidase complex (1%; Vector Laboratories) in 0.05M Tris-buffered saline (TBS) with 0.05% Triton X overnight at 4°C. After washing in TBS, sections were reacted with a mixture of 3,3'-diaminobenzidine tetrahydrochloride (0.02%), nickel ammonium sulfate (0.3%) and H_2O_2 (0.001%) in TBS. Then, sections were postfixed in 1% OsO_4 in PB containing 7% glucose, rinsed in PB, dehydrated in graded ethanol series, mounted on glass slides, and coverslipped with Epon for observation with a light microscope. Neurolucida system (MicroBrightField) was used for a reconstruction of stained cell.

Results

Three firing subtypes of L5 pyramidal cells

L5 pyramidal cells are heterogeneous in their morphological and physiological properties, and project to multiple subcortical areas. To examine their physiological properties, we obtained whole-cell recordings from frontal L5 pyramidal cells. L5 pyramidal cells did not fire spontaneously at the resting membrane potential. During depolarizing current pulse injections, L5 pyramidal cells displayed distinct patterns of spike discharge that were used to classify L5 pyramidal cells into three subtypes (Fig. 1*A*). One class of L5 cell reduced firing frequencies of spike trains during current pulse injection [fast spike frequency adaptation (FA) type (Fig. 1*A*, right traces)], whereas the other cells showed repetitive spike discharges with relatively steady spike frequencies during the current pulse injection [slow spike frequency adaptation (SA) type (Fig. 1*A*, left traces)]. In cells fired repetitively during the entire period of the current pulse, some of them showed initial burst (doublet) spikes at the beginning of the spike trains [Fig. 1*A*, asterisk and inset; slow spike frequency adaptation with initial doublet firing (SA-d) type; middle traces]. From firing frequencies (f) calculated from the first, second, seventh, and shortest interspike intervals [f1, f2, and f7 (Fig. 1*C*, inset) during the current pulse injection (amplitude, 500pA; duration, 1 s)] in individual cells, we obtained the burst (f1/f2), the adaptation index (f7/f2), and the maximum frequency. Shown in Figure 1*B* is the relation between the maximum firing frequency and the adaptation index obtained for L5 pyramidal cells including all cells in which we examined the specificity of connections from L2/3 pyramidal cells. Thus, we quantitatively identified three non-overlapped firing subtypes of L5 pyramidal cell. The burst index of SA-d type cells was significantly higher value than those found in SA and FA type cells (Fig. 1*C*, left histogram) (1.59 ± 0.46, 7.42 ± 3.36, and 2.14 ± 0.66, for SA, SA-d, and FA type, respectively, $n = 150$ for each subtype, $p < 0.01$). The adaptation index of FA type cells was lower than for those of other types (Fig. 1*C*, right histogram) (0.89 ± 0.16, 0.83 ± 0.28, and 0.1 ± 0.12, for SA, SA-d, and FA type, respectively, $n = 150$ for each subtype, $p < 0.01$). All three subtypes of L5 pyramidal cell showed a prominent voltage sag, a sign of the activation of h-current (McCormick and Pape, 1990), in response to negative current pulse injections (Fig. 1*A*, bottom traces). However, among three pyramidal subtypes, FA type cells had significantly larger voltage sag (Table 1) ($p < 0.01$). We also found significant differences in other physiological parameters including resting membrane potentials, input resistance, mean spike frequencies calculated with the exception of f1 (average frequency), and maximum spike frequency between L5 pyramidal subtypes (Table 1).

Pyramidal cells with poorly developed apical tufts were found to be FA type cells, whereas those with dense tufts were physiologically classified as SA or SA-d type cells (Fig. 1*A*). In the frontal cortex, L5 pyramidal cells have been divided into two major projection types: those innervating both sides of the striatum: crossed corticostriatal (CCS) cells, and corticopontine (CPn)

cells that extend their axons to pontine nuclei (Cowan and Wilson, 1994; Levesque et al., 1996; Reiner et al., 2003; Morishima and Kawaguchi, 2006). CCS cells often show the slender sparsely tufted dendritic morphologies whereas CPn cells generally have thick dendritic tufts (Morishima and Kawaguchi, 2006). Correlation between morphologies and projection targets has been also described in the motor cortex (Gao and Zheng, 2004; Hattox and Nelson, 2007). Here we examined the correlation between firing patterns and projection subtypes in the frontal cortex. Recordings from L5 pyramidal cells identified by retrograde fluorescent tracer revealed that most CCS cells (30 of 34 cells) were FA type cells, whereas very few CCS cells showed SA type firing pattern ($n = 4$ of 34). In contrast, CPn cells exhibited SA or SA-d type firing ($n = 29$ and 10 of 39, respectively), but no FA type cells were found (Fig. 1*D*). To further examine the relationship between firing subtypes and their projection sites, we obtained recordings from L5 commissural pyramidal cells projecting to the contralateral frontal cortex (COM cells). It has been shown that a subset of CCS cells projects to the contralateral cortex (Wilson, 1987). Unlike CCS and CPn cells, COM cells showed all three types of firing patterns ($n = 13$, 9, and 16 of 38 cells for SA, SA-d, and FA, respectively) (Fig. 1*D*), suggesting that COM cells contained both CCS and other type of L5 pyramidal cells. These results suggest that the subcortical projection subtype of frontal pyramidal cells is correlated with the intrinsic firing subtype, but also that a firing subtype includes more than one projection subtype. The burst and adaptation indices of the three subtypes of labeled cells were similar with those calculated for nonlabeled L5 pyramidal cells (retrogradely labeled cells: f1/f2, 1.46 ± 0.42 for SA, 6.82 ± 2.74 for SA-d, and 2.07 ± 0.73 for FA; f7/f2, 0.91 ± 0.19 for SA, 0.88 ± 0.31 for SA-d, and 0.074 ± 0.13 for FA). Similar correlations between firing properties and subcortical projection targets have been reported in the mouse motor cortex (Hattox and Nelson, 2007).

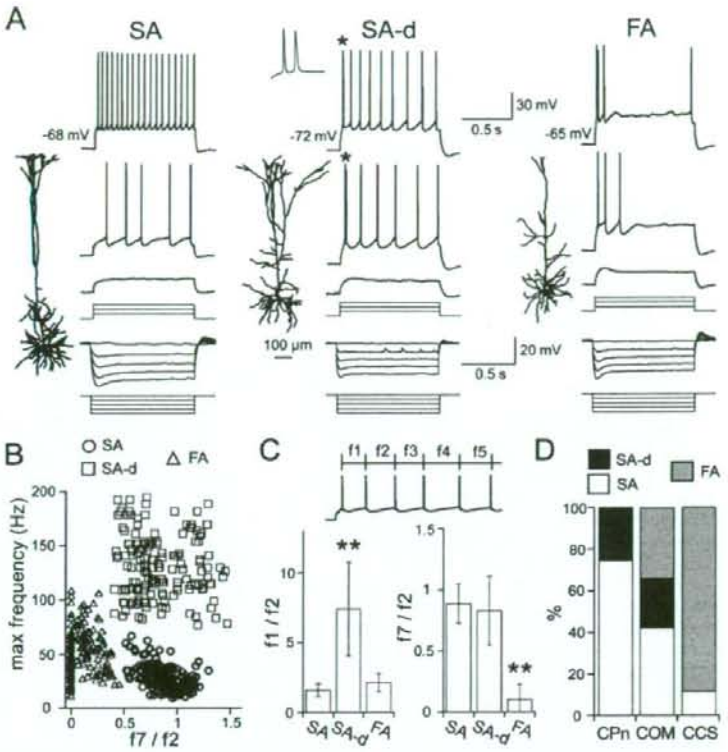

Figure 1. Three firing subtypes of L5 pyramidal cells and their correlation with projection targets. ***A***, Dendritic reconstructions and voltage responses to current injections in SA, SA-d, and FA type L5 pyramidal cells (pulse duration, 1 s; amplitude, from −400 to +500 pA in 100pA steps). Asterisk indicates initial doublet spikes. Inset in SA-d, initial doublet (*) at an expanded time scale and reduced voltage scale. ***B***, Distribution of the relation between maximum spike frequency and the adaptation index (f7/f2) obtained from spike trains generated by current injection (500pA) in three L5 pyramidal subtypes ($n = 183$, 161, and 180, for SA, SA-d, and FA type cell, respectively). Spike frequency (f) was calculated from each interspike interval (see inset in ***C***). Note that three clusters are readily identified by the two firing parameters. ***C***, Comparisons of f1/f2 (burst index) and f7/f2 (adaptation index) between SA, SA-d, and FA type pyramidal subtypes ($n = 150$, respectively). Data are means ± SD; $^{**}p < 0.01$. ***D***, Proportion of firing subtypes among CPn ($n = 39$), COM ($n = 38$) and CCS ($n = 39$) cells identified by retrograde fluorescent tracers.

Detection of synaptic inputs by glutamate puff stimulation

Focal glutamate stimulation to induce action potentials in the cells located restricted area has been widely used to analyze synaptic connections in cortical networks (Schubert et al., 2003; Shepherd and Svoboda, 2005; Shepherd et al., 2005; Yoshimura and Callaway, 2005; Yoshimura et al., 2005). Focal glutamate stimulation allows us to test functional connections to a single recording cell from a large number of cells, individually. To investigate the specificity of synaptic connections from L2/3 to L5 pyramidal cells, we also took advantage of the glutamate stimulation to induce action potentials in L2/3 pyramidal cells. Glutamate was focally applied through the glass pipette placed nearby the soma of L2/3 pyramidal cell aimed to trigger the spike.

Whole-cell or cell-attached recordings were obtained from L2/3 pyramidal cells to examine whether this method reliably induces spikes in the cell (Fig. 2*A*). Although L2/3 pyramidal cells do not fire spontaneously, observed at either cell-attached or whole-cell mode, in the slice preparation, a focal puff of glutamate (1 mM, 50 ms; 5–10 psi) reliably evoked a single spike in L2/3 pyramidal cells when the puff pipette was placed very close to the soma (Fig. 2*A*, upper trace). The latency of spike measured from the glutamate puff onset to the spike peak was 60.1 ± 20.6 ms ($n = 20$). The SD of delays for individual stimulations, representing the variability of the spike timing, was 8.4 ± 4.1 ms. Spikes disappeared when the pipette was moved slightly away from the soma (Fig. 2*A*, lower trace). Glutamate-induced spikes were completely abolished when puff pipettes were positioned 9.8 ± 2.7 μm away from the soma (Fig. 2*B*). To examine the single cell stimulation selectivity by glutamate puff, we obtained recordings from two close neighboring L2/3 pyramidal cells with whole-cell or cell-attached mode, while applying glutamate to either of the two cells. We found that glutamate-puff application evoked a single spike only in one cell that we selected, but not in the other

Table 1. Basic intrinsic membrane properties and EPSCs to L5 pyramidal subtypes

cell type	Vrest (mV)	Ri (MΩ)	Max frequency (/s)	Average frequency (/s)	Vsag (mV)	EPSCs from L2/3 amplitude (pA)	EPSCs from L2/3 rise time (ms)	EPSCs from L2/3 decay (ms)	EPSCs from L5 amplitude (pA)	EPSCs from L5 rise time (ms)	EPSCs from L5 decay (ms)
SA	-68.4 ± 3.4	72.3 ± 19.7	26.9 ± 11.4	15.1 ± 7.4	4.8 ± 1.6	10.7 ± 4.4	3.0 ± 0.9	23.2 ± 7.2	11.3 ± 8.3	2.4 ± 0.5	18.8 ± 8.1
SA-d	-70.0 ± 3.2	81.2 ± 19.7	131.1 ± 28.7	15.5 ± 4.0	4.6 ± 1.2	11.9 ± 4.7	2.6 ± 0.5	22.2 ± 6.3	14.4 ± 14.4	2.7 ± 0.9	20.7 ± 6.7
FA	-67.7 ± 4.8	103.2 ± 29.9	51.9 ± 20.7	13.5 ± 4.1	6.1 ± 1.6	13.2 ± 6.6	3.0 ± 0.9	23.0 ± 5.2	11.9 ± 5.2	2.2 ± 0.7	21.1 ± 4.8
	SA, FA **∨ SA-d	FA **∨ SA-d **∨ SA	SA-d **∨ FA **∨ SA	SA, SA-d *∨ **∨ FA	FA **∨ SA, SA-d						
				*<0.01, *<0.05		n = 11 for SA n = 10 for SA-d n = 10 for FA			n = 25 for SA n = 18 for SA-d n = 12 for FA		
	n = 150 for individual types										

Values are given as mean ± SD. Max frequency, Maximum spike frequency; Ri, input resistance; Vrest, voltage rest; Vsag, voltage sag.

cell (Fig. 2*C*) (n = 12 cell-pairs). Thus, glutamate puff stimulation can selectively induce a single spike in individual L2/3 pyramidal cells.

To examine whether L2/3 pyramidal cell stimulation by glutamate puff can evoke EPSCs in L5 pyramidal cells, we obtained whole-cell recordings from L5 pyramidal cells while puff-applying glutamate to L2/3 pyramidal cells. If a stimulated L2/3 pyramidal cell has synaptic connections with a recorded L5 pyramidal cell, we would detect EPSCs at relatively constant timings after the glutamate puff because of stable spike triggering in the L2/3 pyramidal cell by the stimulation (Fig. 2). We applied glutamate to individual L2/3 pyramidal cells at least 10 times at every 3 s. As expected, EPSCs were evoked at relatively constant latencies among the trials by L2/3 pyramidal cell stimulation (Fig. 2*D*). After EPSC detection by glutamate puff, we obtained whole-cell recordings from the glutamate-stimulated L2/3 pyramidal cell to confirm monosynaptic connections to the recorded L5 pyramidal cell (Fig. 2*E*). We confirmed monosynaptic connections in nearly 90% of connections detected by glutamate puff (30 of 34 pairs). We did not obtain reciprocal connections from L5 to L2/3 pyramidal cells in these cell pairs. Some glutamate puffs induced long lasting inward currents clearly distinguished from EPSCs. Those were probably induced by direct dendritic stimulation of recorded L5 pyramidal cells, because the amplitude and the duration of inward currents were dependent on the intensity and the duration of the puff stimulation (data not shown). These results indicate that focal glutamate stimulation allows testing for monosynaptic connections between cortical cells.

Connection properties from L2/3 to L5 pyramidal cells

By combining glutamate stimulation to L2/3 pyramidal cells and whole-cell recordings, we examined the synaptic connection properties from L2/3 to L5 pyramidal subtypes. First, the connection probability from L2/3 to L5 pyramidal cells was compared among the physiologically identified L5 pyramidal cell subtypes. The connection probability from L2/3 to individual L5 pyramidal cells was calculated from the number of stimulated L2/3 cells that induced synaptic inputs and the total number of L2/3 cells stimulated with glutamate during the recording. Stimulated L2/3 cell number for each L5 pyramidal cells was 23.7 ± 7.8 (ranged from 15 to 50). The connection probability from L2/3 cells to L5 SA and SA-d cells was 0.191 ± 0.093 and 0.196 ± 0.092, respectively (n = 117 and 98 for SA and SA-d). FA type L5 pyramidal cells, however, received synaptic inputs from L2/3 pyramidal cells with a lower connection probability than other L5 subtypes (p = 0.105 ± 0.062, n = 92, $p < 0.01$) (Fig. 2*F*).

To examine for functional differences in the synaptic connections from L2/3 to L5 pyramidal subtypes, we compared the kinetics and frequency characteristics of unitary EPSCs obtained from cell pairs of L2/3 and L5 pyramidal cells by dual whole-cell recordings. The amplitude of EPSCs evoked by a single spike in the L2/3 cell varied between cell pairs. No significant difference was found in the mean amplitude, rise time, and decay of EPSCs between L5 pyramidal subtypes (Table 1). The paired-pulse ratio of the second to first EPSCs amplitudes was calculated from responses evoked by presynaptic spikes delivered at 10 Hz. To avoid the error of analysis (Kim and Alger, 2001), we calculated the ratio as the mean amplitude of the second response divided by that of the first. Both paired-pulse facilitation and depression were observed in all L5 pyramidal subtypes. Shown in Figure 3*A* is a relation between the mean amplitude and the paired-pulse ratio of EPSCs. The paired-pulse ratio depended on the EPSCs amplitude; that is, paired-pulse depression was found more often in connections generating large EPSCs whereas paired-pulse facilitation was observed in connections generating small EPSCs. A similar relationship between the amplitude of EPSCs and paired-pulse ratio has been reported in the hippocampus (Debanne et al., 1996).

For comparison, we investigated the synaptic connection property between L5 pyramidal cells by dual whole-cell recordings. We tested connections between L5 pyramidal cells in 493 cell pairs and found that the connection probabilities from presynaptic SA cells were 0.063 (to other SA, 12/107 cell-pairs), 0.04 (to SA-d cells, 5/125 cell-pairs), and 0.049 (to FA cells, 3/61 cell-pairs). For presynaptic SA-d cells, connection probabilities were 0.056 (to SA, 7/125 cell-pairs), 0.081 (to other SA-d, 9/62 cell-pairs), and 0.032 (to FA, 2/62 cell-pairs). Connection probabilities from presynaptic FA cells were 0.1 (to SA, 6/60 cell-pairs), 0.065 (to SA-d, 4/62 cell-pairs), and 0.053 (to FA, 8/76 cell-pairs). For the same subtype cell pairs, we considered the direction and the reciprocity of connections. The connection probabilities from FA type to SA or SA-d type tend to be higher than the other direction (i.e., from SA or SA-d to FA type cell). Reciprocal connections were found only in SA/SA and SA-d/SA-d type cell pairs. We note that these connection probabilities were obtained from cell-pairs of L5 pyramidal subtypes classified by firing patterns. It has been shown that connections between L5 pyramidal projection subtypes are direction selective (Morishima and Kawaguchi,

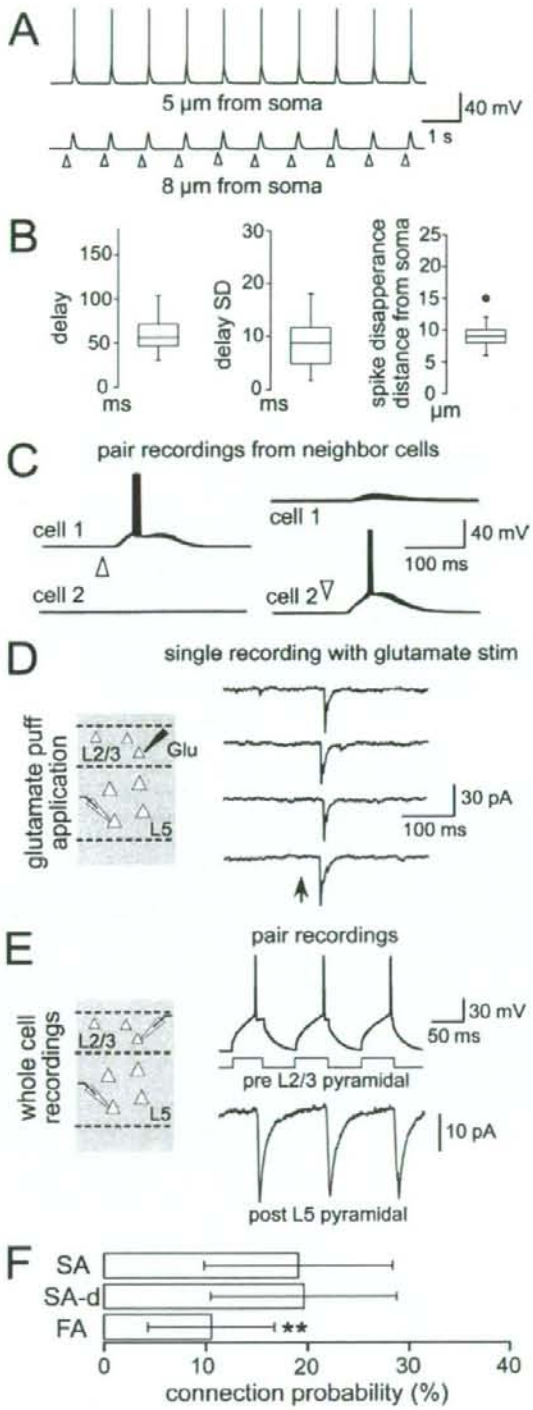

Figure 2. EPSC induction in L5 cells by glutamate puff stimulation to L2/3 pyramidal cells. ***A***, Responses to glutamate puff applications in a L2/3 pyramidal cell. The puff pipette was positioned to 5 μm (top trace) or 8 μm (bottom trace) away from the recorded soma. Arrowheads denote timing of glutamate puff-application (duration, 50 ms). ***B***, Box plot summaries of data for means and SDs of spike induction latencies from the puff onset to the spike peak calculated for individual cells, and the minimum distances from the soma to the pipette that completely eliminate spike production (n = 20 cells; 12 cells in whole-cell and 8 cells in cell-attached modes). ***C***, Recordings from two close neighboring L2/3 pyramidal cells while applying glutamate to either of the two cells. Arrowhead indicates the timing of glutamate puff-application. Ten traces were superimposed. ***D***, Synaptic inputs were detected in L5 pyramidal cells by glutamate puff stimulation to L2/3 pyramidal cells. Arrow indicates glutamate puff onset. ***E***, Verification of EPSC induction by glutamate puff by following dual whole-cell recordings from the stimulated L2/3 cell in addition to the L5 cell. Monosynaptic connections were confirmed in 30 of 34 cases. ***F***, Interlaminar connection probabilities from L2/3 to L5 pyramidal subtypes (n = 117, 98, and 92 for SA, SA-d, and FA type). Data are presented as means ± SD; $^{**}p < 0.01$.

2006). As shown in Figure 1*D*, COM cells exhibited all three firing subtypes, indicating that one firing subtype includes several projection subtypes of L5 pyramidal cells. The kinetics of unitary EPSCs to L5 pyramidal subtypes was independent of postsynaptic cell subtypes (Table 1). Similarly, no significant differences were found in EPSCs kinetics between L2/3 to L5 and L5 to L5 connections. We also examined short-term synaptic plasticity for EPSCs generated from connections between L5 pyramidal cells, and observed both paired-pulse depression and facilitation in all subtypes. Again, a similar relationship between the paired-pulse ratio and EPSCs amplitude in L2/3 to L5 connections was observed in connections between L5 pyramidal cells (Fig. 3*B*). These results suggest that synaptic properties of connections from L2/3 to L5 pyramidal cells are not distinct from those from L5 to L5 pyramidal cells.

Next, we investigated depth distribution of presynaptic L2/3 cells to L5 pyramidal cells. The somatic position of presynaptic L2/3 and postsynaptic L5 cells was measured vertically from the border between layer 1 and layer 2. Shown in Figure 4 is the relation between depth location of EPSC induced L2/3 and postsynaptic L5 cells in glutamate puff stimulation experiments. Both SA and SA-d type L5 pyramidal cells received synaptic inputs from the entire depth of L2/3, whereas EPSC induction in FA type L5 cells was dependent on the location of their somata. Stimulation of L2/3 cells located in the upper part of L2/3 tended to induce EPSCs in FA type cells localized to the upper areas of L5. In contrast, FA type cells located in the lower part of L5 received inputs from lower L2/3 cells. Thus, interlaminar depth correlation between presynaptic and postsynaptic pyramidal cells was found in FA type cells ($p < 0.01$). Together, the subtype differences in connection probability and interlaminar connection topography suggest the existence of multiple different synaptic pathways from L2/3 to L5 cells.

Divergence selectivity from L2/3 to L5 pyramidal subtypes

Pyramidal cells in one layer innervate cells in other layers selectively according to connectivity of the recipient or sender pyramidal cells (Shepherd and Svoboda, 2005; Song et al., 2005; Yoshimura et al., 2005; Kampa et al., 2006). The connection probability from a single cell to two postsynaptic cells in another layer is higher when two recipient cells have connections with each other, suggesting the existence of segregated cortical pathways dependent on connectivity of the recipient layer (Yoshimura et al., 2005; Kampa et al., 2006). However, it remains unknown whether there exist functional channels dependent on pyramidal subtypes in the recipient layer.

To address this, we obtained dual whole-cell recordings from pairs of closely located L5 pyramidal cells with combination of same or different subtypes, while stimulating L2/3 pyramidal cells with glutamate (Fig. 5*A*). The distances between the somata of L5

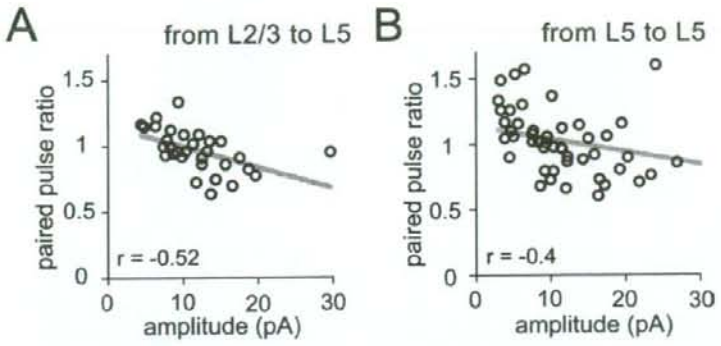

Figure 3. Synaptic frequency characteristics depend on the EPSC amplitude. ***A***, ***B***, Relationship between the mean EPSC amplitude and the paired pulse ratio in L2/3 to L5 connections ($n = 31$) in ***A*** and L5 to L5 connections ($n = 49$) in ***B***. Ten to twenty recordings of EPSCs evoked by two successive presynaptic spikes (10 Hz) were averaged in individual connections. The paired pulse ratio was calculated by the mean of the second response divided by the mean of the first EPSC amplitude.

cell pairs were typically within 50 μm in both the horizontal and vertical directions. If both L5 neurons receive synaptic inputs from the same L2/3 pyramidal cell, synchronous EPSCs should be observed in both L5 cells by glutamate stimulation (Shepherd and Svoboda, 2005; Yoshimura and Callaway, 2005; Yoshimura et al., 2005). After determining the firing types and synaptic connectivity between two L5 pyramidal cells (Fig. 5*B*), we examined common input probability that two L5 cells receives synchronous inputs from L2/3 cells. In some L5 cell pairs, glutamate stimulation induced simultaneous EPSCs in both L5 cells. These synchronous EPSCs were observed stably in both cells at relatively constant latencies in multiple stimulus trials, suggesting excitatory inputs from the same presynaptic cell (Fig. 5*C*, right traces). Glutamate stimulation of some other L2/3 cells induced EPSCs in either of the two L5 cells (Fig. 5*C*, left traces). We calculated the common input probability for each pair of L5 cells by dividing the number of glutamate-stimulated L2/3 cells that induced simultaneous EPSCs in both L5 cells by total number of glutamate-stimulated L2/3 cells (see supplemental information, available at www.jneurosci.org as supplemental material).

The connection probabilities from L2/3 to L5 pyramidal cells depended on the subtypes of postsynaptic L5 pyramidal cells (Figs. 2*F*; 5*D*, upper box). To compare the common input probability among L5 pyramidal subtypes, we normalized common input probabilities for different postsynaptic cell types relative to the probabilities expected for nonselective innervation to two L5 cells (Fig. 5*D*, lower box). The hypothetical common input probability in nonselective cases was calculated by $p_1 \times p_2$. The p_1 and p_2 are the probabilities that L5 cell receives inputs from a given L2/3 cells, taking different values determined experimentally for the different L5 subtypes (i.e., $p = 0.191$, 0.197, and 0.105, for SA, SA-d, and FA cells, respectively).

To distinguish between the effects of subtype combination and intralaminar connectivity between two L5 cells, we first compared the common input probability between unconnected L5 cell pairs, using the ratio of the observed probability and the expected probability assuming nonselective innervations (Fig. 5*E*). The relative probability was close to one in cell pairs of different L5 pyramidal subtypes. However, when both L5 cells were of the same subtype, the common input probability ratio was significantly higher than those in the different subtype pairs (2.57 ± 0.85, 2.5 ± 0.54, and 2.79 ± 0.74 for SA/SA, SA-d/SA-d, and FA/FA cell pairs, respectively). These results suggest that L2/3 pyramidal cells innervate L5 pyramidal cells selectively depending on the subtype of the L5 target neurons.

We, next, examined whether the synaptic connectivity between L5 cells influences the common input probability from L2/3. We compared the common input probabilities between connected and unconnected cell pairs separately in pairs consisting of cells of the same (homo) and different (hetero) L5 subtypes. For connected cell pairs, we adopted L5 cell pairs with both one way and reciprocally connections. Connections from L2/3 to L5 pyramidal cells were highly selective when L5 cells were of the same physiological subtype and had connections between them (Fig. 6*A*). The common input probability ratio was 3.76 ± 0.88 for connected pairs of the same subtype, higher than one for unconnected cell pairs of the same subtype (2.59 ± 0.68, $p < 0.01$). However, in pairs of different L5 subtypes, the common input probability did not depend on connectivity between L5 cells (1.32 ± 0.34 for connected pairs, 1.38 ± 0.33 for unconnected pairs, $p = 0.556$). Even if we included cases with no common inputs, but EPSCs in both L5 cells, common input probabilities between two L5 pyramidal cells showed similar specificity dependent on their subtype combination and connectivity (supplemental Fig. 1, available at www.jneurosci.org as supplemental material).

Discussion

In this study, we examined the specificity of excitatory connections from L2/3 to L5 pyramidal subtypes, classified by their firing properties. We found that L5 pyramidal cells received synaptic inputs from L2/3 pyramidal cells with different connection probability and intralaminar location of presynaptic and postsynaptic cell soma, in a subtype-dependent manner. Moreover, we showed that L5 pyramidal cells received common excitatory inputs from L2/3 pyramidal cells dependent on firing subtypes of L5 cells and synaptic connectivity between them; higher probabilities to L5 cell pairs of the same subtype than the different one; and highly selective to connected L5 cell pairs of same subtype, but not of different firing patterns (Fig. 6*B*). Our results suggest that excitatory connections from L2/3 to L5 pyramidal cells form subnetworks dependent on L5 pyramidal subtypes.

L5 pyramidal cells project to various subcortical structures (Wise and Jones, 1977). Recent studies have found correlations between the dendritic morphologies of L5 pyramidal cells and their extracortical axonal targets (Reiner et al., 2003; Gao and Zheng, 2004; Morishima and Kawaguchi, 2006; Hattox and Nelson, 2007). Furthermore, a group of L5 pyramidal cells projecting to the same extracortical target share common electrophysiological properties (Hattox and Nelson, 2007). Here, we have quantitatively confirmed the relationship between firing patterns of frontal L5 pyramidal cells and their subcortical projection patterns to contralateral striatum or ipsilateral pontine nuclei. These observations suggest that the cortical output to subcortical areas is conveyed by target-specific groups of pyramidal cells with distinct morphological and electrophysiological characteristics. Frontal L5 pyramidal cells projecting to contralateral cortex, however, exhibited all three firing subtypes (Fig. 1*D*), suggesting that one firing subtype contains multiple projection subtypes. In

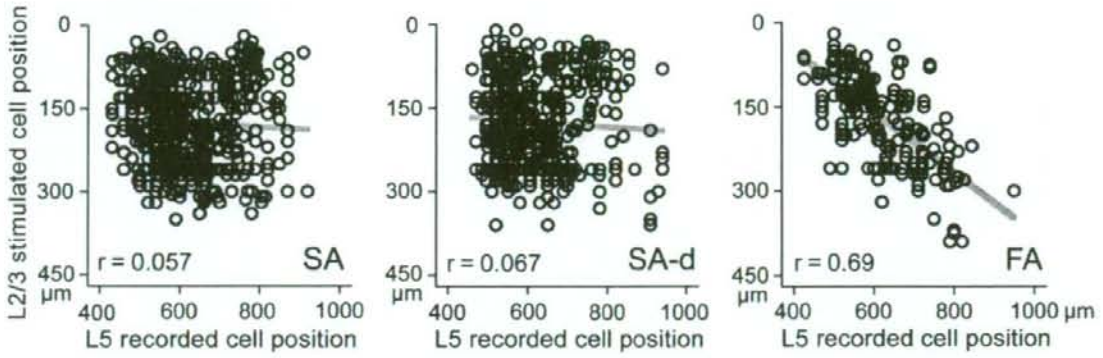

Figure 4. Interlaminar connection maps to L5 pyramidal subtypes. Relationship between somatic locations of presynaptic L2/3 cells and of postsynaptic L5 pyramidal cells varied among L5 firing subtypes. Cell positions were measured as the vertical distance from the L1 and L2/3 border. Regression lines indicate the interlaminar topographic connections to FA type L5 cells, but not to SA or SA-d cells.

the parietal associative and visual cortical area, L5 pyramidal cells projecting to the superior colliculus or contralateral cortex show similar firing properties (Christophe et al., 2005). Together, correlation between the firing properties and axonal projections of pyramidal cell differs according to cortical areas and extracortical targets.

We classified firing patterns of pyramidal cells to three types based on initial burst firing and the spike frequency adaptation during current pulse injection. Spike discharge patterns to depolarizing current pulses have been studied for a long time. In a way similar to ours, several studies have identified three or more groups of L5 pyramidal cells by *in vitro* or *in vivo* recordings from various cortical areas and species (Connors et al., 1982; Nuñez et al., 1993; Schwindt et al., 1997; Dégenètais et al., 2002; Schubert et al., 2006; Chang and Luebke, 2007). It has been shown that burst firing of pyramidal cells is influenced by many factors, such as intracellular and extracellular Ca^{2+} concentration (Friedman and Gutnick, 1989; Su et al., 2001; Golomb et al., 2006) and prolonged exposure to anesthesia (Christophe et al., 2005). The SA-d type cells, described here, which fired an initial doublet followed by trains of single spikes, may correspond to intrinsically bursting (IB) cells that have been described as fired with an initial burst of 3 and more spikes (Connors et al., 1982; Agmon and Connors, 1992; Nuñez et al., 1993; Gray and McCormick, 1996). However, we did not find the morphological or axonal target differences between SA and SA-d type cells, as has been described between regular spiking and IB pyramidal cells in the somatosensory cortex (Schubert et al., 2006). Regardless, the connection specificity dependent on SA and SA-d types suggests that these cell types play distinct functional roles in cortical circuits.

We found the connection probability from L2/3 to FA type L5 cells was lower than the probability of connections onto SA or SA-d cells. This finding corresponds well with a previous report that L5 pyramidal cells with thick tufted apical dendrites (as found here in SA and SA-d cells) receive more frequent inputs from L2/3 pyramidal cells than those with slender apical dendrites (Thomson and Bannister, 1998). In the barrel cortex, however, both types of L5 pyramidal cells received inputs from L2/3 pyramidal cells with similar connection probabilities (Schubert et al., 2001), suggesting the differences between cortical areas in connection probabilities from L2/3 to L5 pyramidal subtypes. Although L5 pyramidal cells make axonal contacts mainly on basal dendrites of other L5 pyramidal cells, L2/3 pyramidal cells are likely to innervate apical dendrites of L5 pyramidal cells (Letzkus et al., 2006; Morishima and Kawaguchi, 2006; Sjöström and Häusser, 2006). The differences in apical dendritic arborization between pyramidal subtypes (Morishima and Kawaguchi, 2006), may contribute to differences in connection probability from L2/3 to L5 pyramidal subtypes. In addition, FA type cells received excitatory inputs from L2/3 cells in a topographic manner, depending on the depth of their soma in the layer. Given that a similar relationship was not seen in SA or SA-d cells, it is unlikely that this result is reflective of distance-dependent changes in connection probability, but rather reflects the functional topographical relationship between different subsets of L2/3 and L5 FA cells. It has previously been shown that L5 pyramidal cells projecting to different subcortical targets distribute unevenly within the layer (Wise and Jones, 1977; Killackey et al., 1989; Reiner et al., 2003). Thus, different interlaminar excitatory sources dependent on L5 subtypes may form further specialized subnetworks for particular subcortical targets.

Regardless of differences in connection probabilities and presynaptic cell locations, we found no obvious differences in synaptic properties from L2/3 to L5 pyramidal subtypes and connections between L5 subtypes. Both paired-pulse facilitation and depression, reflecting release probabilities of presynaptic terminals (Debanne et al., 1996), were found in all L5 subtypes. Optical quantal analysis revealed large variability of the release probability at synaptic boutons onto different postsynaptic pyramidal cells, but release probability of different boutons contacting to the same postsynaptic cells varied little (Koester and Johnston, 2005). Although frequency characteristics of synaptic transmission from pyramidal cell to inhibitory interneurons depend on the presynaptic pyramidal subtypes (Angulo et al., 2003), the frequency characteristics of connections between pyramidal cells may appear to be independent of subtype, and may rather be related to the plastic change of unitary connections.

The specificity of connections between cortical pyramidal cells has been elegantly investigated in studies using uncaged glutamate photostimulation and multiple recordings (Shepherd and Svoboda, 2005; Song et al., 2005; Yoshimura et al., 2005; Kampa

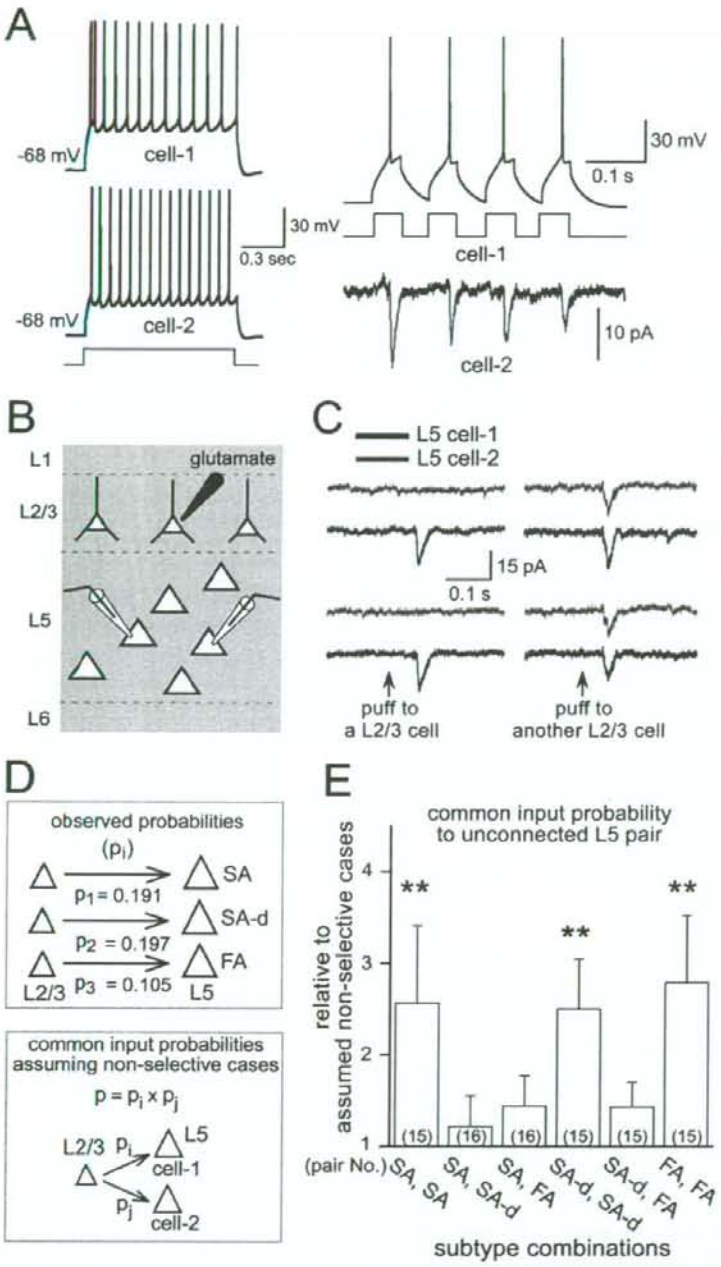

Figure 5. Divergent connection selectivity from L2/3 to L5 pyramidal subtypes. ***A***, Dual whole-cell recordings from L5 pyramidal cells. Left, Identification of firing subtypes (cell-1, SA-d; cell-2, SA). Right, EPSCs in cell-2 induced by cell-1 spikes. ***B***, Divergence connections to two L5 pyramidal subtypes tested by L2/3 cell stimulation by glutamate puff. ***C***, EPSC induction in two L5 cells. Left, EPSCs observed only in one cell; right, common inputs induced by L2/3 cell stimulation. ***D***, Top box, Observed connection probabilities from L2/3 to L5 pyramidal subtypes. Bottom box, Calculation of common input probabilities assuming nonselective innervations. ***E***, Probabilities that two L5 pyramidal cells share common inputs from a L2/3 cell in the case of unconnected L5 pairs, relative to those assuming nonselective cases. The common input probabilities were compared between subtype combinations of L5 pairs. Data are means ± SD; $^{**}p < 0.01$.

et al., 2006). However, these studies have not considered pyramidal cell heterogeneity in firing properties, morphologies, and subcortical targets. The glutamate puff stimulation used here can excite cells in a more restricted area (within 10 μm from the pipette tip) than the previous uncaging photostimulation (Dantzker and Callaway, 2000; Shepherd and Svoboda, 2005; Shepherd et al., 2005; Yoshimura and Callaway, 2005; Yoshimura et al., 2005). Using glutamate stimulation, we demonstrated divergence connectional selectivity from L2/3 to two L5 firing subtypes that are correlated with morphology and subcortical targeting. The common input probability obtained here might, however, have been overestimated, because of the limitation of the number of glutamate stimulated L2/3 cells. In addition, to calculate the common input probability, we adopted cell pairs in which we detected synchronous EPSCs during the recordings. These would reflect that the relative common input probabilities in all groups of L5 cell pairs showed >1. In the somatosensory cortex, L5 pyramidal cells receive common inputs from L2/3 pyramidal cells with higher probability than the assumed random cases when L5 pyramidal cells have connections with each other (Kampa et al., 2006). We investigated dependency of the common input probability from L2/3 to two L5 cells on the subtype combination and synaptic connectivity between two postsynaptic L5 cells. Common inputs from L2/3 to L5 cells were highly selective between connected cell pairs of the same subtype, but not different subtypes. Moreover, unconnected cell pairs of the same subtype received common inputs from L2/3 cells with higher probability than did cell pairs of different subtypes regardless of whether those cells were synaptically connected or not. Our results suggest that intralaminar neuron subtyping should be taken into account when analyzing interlaminar connections.

In the present study, we showed synaptic pathways from L2/3 to L5 pyramidal cells are differentiated according to L5 pyramidal firing subtypes. Firing properties of L5 pyramidal cells were correlated with particular extracortical targets (Fig. 1*D*) (Hattox and Nelson, 2007). Together, these observations suggest that the L2/3 to L5 excitatory pathway is composed of functionally segregated channels corresponding to projection systems to some extracortical targets. Interactions between different L2/3 to L5 excitatory subnetworks would be performed on connections between pyramidal cells in the same

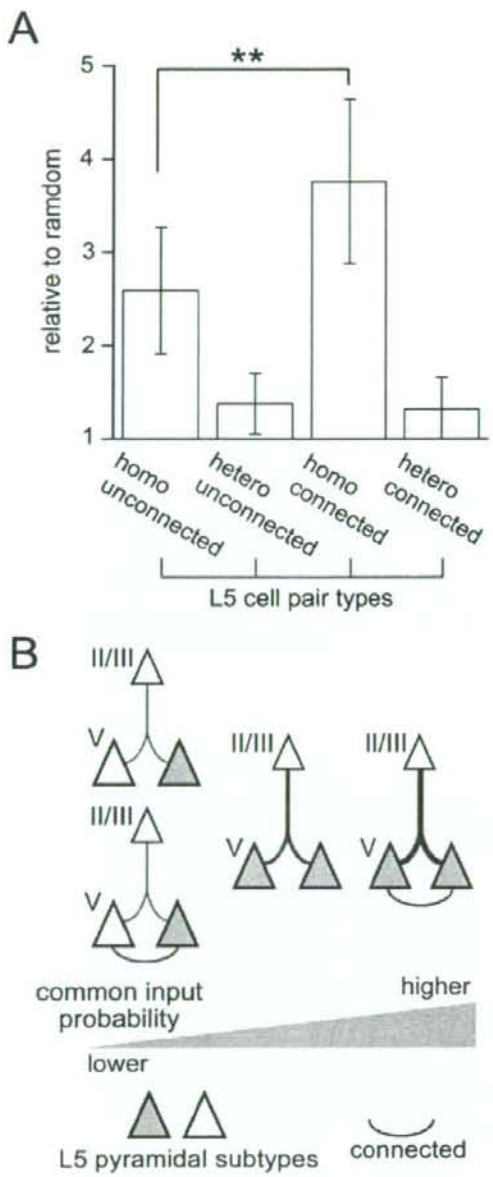

Figure 6. Effect of subtype homology and connectivity between L5 cells on connection selectivity from L2/3 pyramidal cells. ***A***, Common input probabilities to two L5 cells compared between the same (homo) and different (hetero) subtype pairs ($n = 45$ and 47 pairs, respectively), and between connected ($n = 15$) and unconnected pairs ($n = 15$). Data are means ± SD; $^{**}p < 0.01$. ***B***, Schematic diagram of interlaminar divergence selectivity from L2/3 to L5 pyramidal cells. Line thickness represents connection probabilities. Open and dark triangles indicate different pyramidal subtypes.

layer (L5 and L2/3). Moreover, the observation that connections between L5 projection subtypes are differentiated in a direction preference manner (Morishima and Kawaguchi, 2006) suggests the hierarchy among different L2/3 to L5 subnetworks for particular subcortical targets.

References

Agmon A, Connors BW (1992) Correlation between intrinsic firing patterns and thalamocortical synaptic responses of neurons in mouse barrel cortex. J Neurosci 12:319–329.

Angulo MC, Staiger JF, Rossier J, Audinat E (2003) Distinct local circuits between neocortical pyramidal cells and fast-spiking interneurons in young adult rats. J Neurophysiol 89:943–953.

Bureau I, von Saint Paul F, Svoboda K (2006) Interdigitated paralemniscal and lemniscal pathways in the mouse barrel cortex. PLoS Biol 4:e382.

Chagnac-Amitai Y, Luhmann HJ, Prince DA (1990) Burst generating and regular spiking layer 5 pyramidal neurons of rat neocortex have different morphological features. J Comp Neurol 296:598–613.

Chang YM, Luebke JI (2007) Electrophysiological diversity of layer 5 pyramidal cells in the prefrontal cortex of the rhesus monkey: in vitro slice studies. J Neurophysiol 98:2622–2632.

Cho RH, Segawa S, Mizuno A, Kaneko T (2004) Intracellularly labeled pyramidal neurons in the cortical areas projecting to the spinal cord. I. Electrophysiological properties of pyramidal neurons. Neurosci Res 50:381–394.

Christophe E, Doerflinger N, Lavery DJ, Molnár Z, Charpak S, Audinat E (2005) Two populations of layer V pyramidal cells of the mouse neocortex: development and sensitivity to anesthetics. J Neurophysiol 94:3357–3367.

Connors BW, Gutnick MJ, Prince DA (1982) Electrophysiological properties of neocortical neurons in vitro. J Neurophysiol 48:1302–1320.

Cowan RL, Wilson CJ (1994) Spontaneous firing patterns and axonal projections of single corticostriatal neurons in the rat medial agranular cortex. J Neurophysiol 71:17–32.

Dantzker JL, Callaway EM (2000) Laminar sources of synaptic input to cortical inhibitory interneurons and pyramidal neurons. Nat Neurosci 3:701–707.

Debanne D, Guérineau NC, Gähwiler BH, Thompson SM (1996) Paired-pulse facilitation and depression at unitary synapses in rat hippocampus: quantal fluctuation affects subsequent release. J Physiol 491:163–176.

DeFelipe J, Fariñas I (1992) The pyramidal neuron of the cerebral cortex: morphological and chemical characteristics of the synaptic inputs. Prog Neurobiol 39:563–607.

Dégenètais E, Thierry AM, Glowinski J, Gioanni Y (2002) Electrophysiological properties of pyramidal neurons in the rat prefrontal cortex: an in vivo intracellular recording study. Cereb Cortex 12:1–16.

Friedman A, Gutnick MJ (1989) Intracellular calcium and control of burst generation in neurons of guinea-pig neocortex in vitro. Eur J Neurosci 1:374–381.

Gao WJ, Zheng ZH (2004) Target-specific differences in somatodendritic morphology of layer V pyramidal neurons in rat motor cortex. J Comp Neurol 476:174–185.

Golomb D, Yue C, Yaari Y (2006) Contribution of persistent Na^+ current and M-type K^+ current to somatic bursting in CA1 pyramidal cells: combined experimental and modeling study. J Neurophysiol 96:1912–1926.

Gottlieb JP, Keller A (1997) Intrinsic circuitry and physiological properties of pyramidal neurons in rat barrel cortex. Exp Brain Res 115:47–60.

Gray CM, McCormick DA (1996) Chattering cells: superficial pyramidal neurons contributing to the generation of synchronous oscillations in the visual cortex. Science 274:109–113.

Hattox AM, Nelson SB (2007) Layer V neurons in mouse cortex projecting to different targets have distinct physiological properties. J Neurophysiol 98:3330–3340.

Hefti BJ, Smith PH (2000) Anatomy, physiology, and synaptic responses of rat layer V auditory cortical cells and effects of intracellular $GABA_A$ blockade. J Neurophysiol 83:2626–2638.

Kampa BM, Letzkus JJ, Stuart GJ (2006) Cortical feed-forward networks for binding different streams of sensory information. Nat Neurosci 9:1472–1473.

Kawaguchi Y, Kubota Y (1997) GABAergic cell subtypes and their synaptic connections in rat frontal cortex. Cereb Cortex 7:476–486.

Killackey HP, Koralek KA, Chiaia NL, Rhodes RW (1989) Laminar and areal differences in the origin of the subcortical projection neurons of the rat somatosensory cortex. J Comp Neurol 282:428–445.

Kim J, Alger BE (2001) Random response fluctuations lead to spurious paired-pulse facilitation. J Neurosci 21:9608–9618.

Koester HJ, Johnston D (2005) Target cell-dependent normalization of transmitter release at neocortical synapses. Science 308:863–866.

Letzkus JJ, Kampa BM, Stuart GJ (2006) Learning rules for spike timing-dependent plasticity depend on dendritic synapse location. J Neurosci 26:10420–10429.

Lévesque M, Charara A, Gagnon S, Parent A, Deschênes M (1996) Corticostriatal projections from layer V cells in rat are collaterals of long-range corticofugal axons. Brain Res 709:311–315.

Lübke J, Feldmeyer D (2007) Excitatory signal flow and connectivity in a cortical column: focus on barrel cortex. Brain Struct Funct 212:3–17.

Markram H, Toledo-Rodriguez M, Wang Y, Gupta A, Silberberg G, Wu C (2004) Interneurons of the neocortical inhibitory system. Nat Rev Neurosci 5:793–807.

Mason A, Larkman A (1990) Correlations between morphology and electrophysiology of pyramidal neurons in slices of rat visual cortex. II. Electrophysiology. J Neurosci 10:1415–1428.

McCormick DA, Pape HC (1990) Properties of a hyperpolarization-activated cation current and its role in rhythmic oscillation in thalamic relay neurones. J Physiol 431:291–318.

McCormick DA, Connors BW, Lighthall JW, Prince DA (1985) Comparative electrophysiology of pyramidal and sparsely spiny stellate neurons of the neocortex. J Neurophysiol 54:782–806.

Morishima M, Kawaguchi Y (2006) Recurrent connection patterns of corticostriatal pyramidal cells in frontal cortex. J Neurosci 26:4394–4405.

Mountcastle VB (1997) The columnar organization of the neocortex. Brain 120:701–722.

Nuñez A, Amzica F, Steriade M (1993) Electrophysiology of cat association cortical cells in vivo: intrinsic properties and synaptic responses. J Neurophysiol 70:418–430.

Reiner A, Jiao Y, Del Mar N, Laverghetta AV, Lei WL (2003) Differential morphology of pyramidal tract-type and intratelencephalically projecting-type corticostriatal neurons and their intrastriatal terminals in rats. J Comp Neurol 457:420–440.

Schubert D, Staiger JF, Cho N, Kötter R, Zilles K, Luhmann HJ (2001) Layer-specific intracolumnar and transcolumnar functional connectivity of layer V pyramidal cells in rat barrel cortex. J Neurosci 21:3580–3592.

Schubert D, Kötter R, Zilles K, Luhmann HJ, Staiger JF (2003) Cell type-specific circuits of cortical layer IV spiny neurons. J Neurosci 23:2961–2970.

Schubert D, Kötter R, Luhmann HJ, Staiger JF (2006) Morphology, electrophysiology and functional input connectivity of pyramidal neurons characterizes a genuine layer Va in the primary somatosensory cortex. Cereb Cortex 16:223–236.

Schwindt P, O'Brien JA, Crill W (1997) Quantitative analysis of firing properties of pyramidal neurons from layer 5 of rat sensorimotor cortex. J Neurophysiol 77:2484–2498.

Shepherd GM, Svoboda K (2005) Laminar and columnar organization of ascending excitatory projections to layer 2/3 pyramidal neurons in rat barrel cortex. J Neurosci 25:5670–5679.

Shepherd GM, Stepanyants A, Bureau I, Chklovskii D, Svoboda K (2005) Geometric and functional organization of cortical circuits. Nat Neurosci 8:782–790.

Sjöström PJ, Häusser M (2006) A cooperative switch determines the sign of synaptic plasticity in distal dendrites of neocortical pyramidal neurons. Neuron 51:227–238.

Song S, Sjöström PJ, Reigl M, Nelson S, Chklovskii DB (2005) Highly nonrandom features of synaptic connectivity in local cortical circuits. PLoS Biol 3:e68.

Su H, Alroy G, Kirson ED, Yaari Y (2001) Extracellular calcium modulates persistent sodium current-dependent burst-firing in hippocampal pyramidal neurons. J Neurosci 21:4173–4182.

Thomson AM, Bannister AP (1998) Postsynaptic pyramidal target selection by descending layer III pyramidal axons: dual intracellular recordings and biocytin filling in slices of rat neocortex. Neuroscience 84:669–683.

Tsiola A, Hamzei-Sichani F, Peterlin Z, Yuste R (2003) Quantitative morphologic classification of layer 5 neurons from mouse primary visual cortex. J Comp Neurol 461:415–428.

Wilson CJ (1987) Morphology and synaptic connections of crossed corticostriatal neurons in the rat. J Comp Neurol 263:567–580.

Wise SP, Jones EG (1977) Cells of origin and terminal distribution of descending projections of the rat somatic sensory cortex. J Comp Neurol 175:129–157.

Yoshimura Y, Callaway EM (2005) Fine-scale specificity of cortical networks depends on inhibitory cell type and connectivity. Nat Neurosci 8:1552–1559.

Yoshimura Y, Dantzker JL, Callaway EM (2005) Excitatory cortical neurons form fine-scale functional networks. Nature 433:868–873.

Available online at www.sciencedirect.com
ScienceDirect
Neuroscience Research 61 (2008) 143–158
Neuroscience Research
www.elsevier.com/locate/neures

Behavioral and gene expression analyses of *Wfs1* knockout mice as a possible animal model of mood disorder

Tadafumi Kato [a,*], Mizuho Ishiwata [a], Kazuyuki Yamada [b], Takaoki Kasahara [a], Chihiro Kakiuchi [a], Kazuya Iwamoto [a], Koki Kawamura [c], Hisamitsu Ishihara [d], Yoshitomo Oka [d]

[a] *Laboratory for Molecular Dynamics of Mental Disorders, RIKEN Brain Science Institute, Hirosawa 2-1, Wako, Saitama 351-0198, Japan*
[b] *Support Unit for Animal Experiment, RIKEN Brain Science Institute, Wako, Saitama 351-0198, Japan*
[c] *Laboratory for Cell Culture Development, RIKEN Brain Science Institute, Wako, Saitama 351-0198, Japan*
[d] *Division of Molecular Metabolism and Diabetes, Tohoku University Graduate School of Medicine, Sendai, Japan*

Received 21 November 2007; accepted 7 February 2008
Available online 14 February 2008

Abstract

Wolfram disease is a rare genetic disorder frequently accompanying depression and psychosis. Non-symptomatic mutation carriers also have higher rates of depression and suicide. Because *WfS1*, the causative gene of Wolfram disease, is located at 4p16, a linkage locus for bipolar disorder, mutations of *WfS1* were suggested to be involved in the pathophysiology of bipolar disorder. In this study, we performed behavioral and gene expression analyses of *Wfs1* knockout mice to assess the validity as an animal model of mood disorder. In addition, the distribution of *Wfs1* protein was examined in mouse brain. *Wfs1* knockout mice did not show abnormalities in circadian rhythm and periodic fluctuation of wheel-running activity. Behavioral analysis showed that *Wfs1* knockout mice had retardation in emotionally triggered behavior, decreased social interaction, and altered behavioral despair depending on experimental conditions. *Wfs1*-like immunoreactivity in mouse brain showed a similar distribution pattern to that in rats, including several nuclei potentially relevant to the symptoms of mood disorders. Gene expression analysis showed down-regulation of *Cdc42ep5* and *Rnd1*, both of which are related to Rho GTPase, which plays a role in dendrite development. These findings may be relevant to the mood disorder observed in patients with Wolfram disease.

Keywords: Wolframin; Wolfram disease; Depression; Bipolar disorder; DNA microarray; Forced swimming test

1. Introduction

Wolfram disease (Online Mendelian Inheritance in Man [OMIM] 222300) is a rare autosomal recessive neurodegenerative disorder characterized by early-onset diabetes mellitus, progressive optic atrophy, diabetes insipidus, and deafness (Domenech et al., 2006); *WfS1/wolframin* has been identified as the causative gene (Strom et al., 1998; Inoue et al., 1998). Approximately, 60% of the patients with Wolfram disease have mental symptoms, such as severe depression, psychosis, impulsivity, and aggression (Swift et al., 1990). More importantly, carriers of *WfS1* mutations, who are not affected with Wolfram disease, have a 26-fold higher likelihood of psychiatric hospitalization mainly due to depression (Swift and Swift, 2000). The *WfS1* gene locates at 4p16.1 (Strom et al., 1998; Inoue et al., 1998), a replicated linkage locus of bipolar disorder (Ewald et al., 1998, 2002; Detera-Wadleigh et al., 1999). Some studies showed that bipolar disorder with psychosis (Als et al., 2004; Cheng et al., 2006) or suicidal behavior (Cheng et al., 2006) is linked with this locus. These lines of evidence suggested the possible role of *WfS1* mutations in the pathophysiology of bipolar disorder and related phenotypes.

To date, mutation screening of the *WfS1* gene has been reported in 84 patients with bipolar disorder, 54 with major depression, 119 with schizophrenia, 100 suicide victims, 3 with schizoaffective disorder, and several other patients with other psychiatric diagnoses (Ohtsuki et al., 2000; Martorell et al., 2003; Torres et al., 2001; Crawford et al., 2002; Evans et al., 2000). However, none of these patients had mutations causing Worfram disease.

* Corresponding author. Tel.: +81 48 467 6949; fax: +81 48 467 6947.
E-mail address: kato@brain.riken.jp (T. Kato).

0168-0102/$ – see front matter © 2008 Published by Elsevier Ireland Ltd and the Japan Neuroscience Society.
doi:10.1016/j.neures.2008.02.002

Despite the fact that *WfS1* mutations may not be a frequent cause of mental disorders, the mechanism underlying how *WfS1* mutations lead to mental symptoms in patients with Wolfram disease will shed light on the pathophysiology of mood disorders. Mice lacking the *Wfs1* gene might be useful as a genetic animal model of mood disorders.

The symptoms of Wolfram disease resemble those of mitochondrial diseases and, indeed, initial studies suggested mitochondrial dysfunction in Wolfram disease based on mitochondrial DNA (mtDNA) deletions found in patients (Rotig et al., 1993). However, the protein coded by *WfS1* was found to be localized in endoplasmic reticulum (ER) (Takeda et al., 2001; Philbrook et al., 2005). *WfS1* expression was induced by ER stress (Fonseca et al., 2005) or *XBP1* overexpression (Kakiuchi et al., 2006), and disruption of *Wfs1* caused a dysfunctional ER stress response (Fonseca et al., 2005; Riggs et al., 2005; Yamada et al., 2006). Recent studies have provided insight into the function of *WfS1* protein; *WfS1* induces cation channel activity on ER membranes (Osman et al., 2003) and regulates calcium levels in ER (Takei et al., 2006). It also plays a role in stimulus-secretion coupling for insulin exocytosis in pancreatic β cells (Ishihara et al., 2004). Disruption of *Wfs1* increased vulnerability to cell death in the knockout (KO) mice (Ishihara et al., 2004; Philbrook et al., 2005; Riggs et al., 2005; Yamada et al., 2006). In the rat brain, *WfS1* was distributed predominantly in neurons of the so-called limbic system (Takeda et al., 2001). *WfS1* mutations could lead to loss of *WfS1*-expressing neurons in particular brain regions of patients with Wolfram disease, which may underlie progression of mental symptoms.

In this study, we performed behavioral analysis of *Wfs1* KO mice to characterize their behavioral abnormality. We previously developed neuron-specific mutant polymerase γ-transgenic mice (mPolg Tg mice) based on a mitochondrial dysfunction hypothesis of bipolar disorder (Kato and Kato, 2000) and demonstrated that these mice had bipolar disorder-like phenotypes, such as altered circadian rhythm and periodic fluctuation of wheel-running activity (Kasahara et al., 2006). Whether or not the *Wfs1* KO mice show such wheel-running activity was examined. A behavioral test battery was also conducted to search for other behavioral phenotypes. Distribution of *Wfs1* in the brain was examined to search for the neural basis of behavioral alteration. In addition, gene expression analysis was performed to search for the molecular basis of behavioral phenotypes of *Wfs1* KO mice.

2. Experimental procedures

2.1. Generation of Wfs1 KO mice

The methods for the generation of *Wfs1* KO mice have been described elsewhere (Ishihara et al., 2004). In brief, a neomycin-resistance gene was inserted into exon 2 of the *Wfs1* gene in the targeting vector. The targeting vector was injected into 129Sv embryonic stem (ES) cells, and the ES cells with homologous recombination were obtained. By crossing the chimeric mice with C57BL/6J (B6) mice, *Wfs1* heterozygous KO mice were obtained. Genotyping was performed as previously described (Ishihara et al., 2004). The heterozygous KO mice were crossed with the B6 mice for at least eight generations before the analysis. The mice were maintained in a 12-h light:12-h dark cycle, except for several specific experiments as indicated. Wild-type (WT) littermates were used for the control whenever possible. All animal experiments were approved by the local animal experiment committees of RIKEN and Behavioral and Medical Sciences Research Consortium (BMSRC) (Akashi, Japan). Animal experiments were carried out in accordance with the National Institute of Health Guide for the Care and Use of Laboratory Animals. All efforts were made to minimize the number of animals used and their suffering.

2.2. Wheel-running activity

For this analysis, 11 homozygous KO mice (*Wfs1*$^{-/-}$) and 9 WT littermates (*Wfs1*$^{+/+}$) were used. All were males aged 34 weeks at the initiation of the analysis. The groups did not differ significantly in body weight.

The methods for the analysis of wheel-running activity were described in detail elsewhere (Kasahara et al., 2006). In brief, mice were individually housed in cages (width, 24 cm; depth, 11 cm; height, 14 cm) equipped with a steel wheel (width, 5 cm; diameter, 14 cm) (O'Hara & Co., Tokyo, Japan). Wheel-running activity was monitored by measuring the rotation of the wheel (3 counts/1 rotation). Food and water were available ad libitum. The data of initial 7–10 days were omitted from the analysis. Delayed and anticipatory activity indices, referring to the wheel-running activity during the initial 3 h of a light phase and that during the last 3 h of a light phase, were calculated. The periodicity of wheel-running activity was assessed by Lomb-Scargle periodogram (Kasahara et al., 2006).

The Mann–Whitney *U*-test was used for statistical analyses. Significance levels were set at 0.05 (two-tailed; d.f., degree of freedom). The average and standard error of mean (S.E.M.) were presented for each experimental parameter in one group.

2.3. Behavioral analysis: phase I. Screening by a test battery

This analysis was performed at BMSRC (Akashi, Japan). For this analysis, 14 homozygous KO mice (*Wfs1*$^{-/-}$), 14 heterozygous KO mice (*Wfs1*$^{-/+}$), and 13 WT littermates (*Wfs1*$^{+/+}$) were analyzed. All were males aged 12 weeks at the initiation of the behavioral analysis. The analyses were performed in the order of open-field test, startle response and prepulse inhibition test, elevated plus maze, Morris water maze, passive avoidance learning, active avoidance learning, and forced swimming test. After the behavioral test battery, the non-fasting blood glucose level was examined to rule out the possibility that elevated blood glucose levels might affect the results of behavioral analysis. There was no significant difference among the genotypes, consistent with a previous report that there was no apparent increase in blood glucose levels in *Wfs1* KO mice on the B6 background (Ishihara et al., 2004).

2.3.1. Open-field test

A transparent cubic box without a ceiling (30 cm × 30 cm × 30 cm) was placed in a ventilated sound-attenuating chamber. A 40-W white lamp provided room lighting, which was approximately 110 lx on the floor of the chamber. In addition, a fan attached on the upper part of the wall at one end of the chamber presented a masking noise of 45 dB. Two infrared beams were set on each wall 2 cm above the floor with an interval of 10 cm. The total number of successive interceptions of two adjoining beams on each bank was scored as locomotion behavior. The other 12 infrared ray beams were attached 4.5 cm above the floor in 2.5-cm intervals, and the total number of vertical beam interceptions was scored as rearing behavior. Each mouse was allowed to explore freely in the open-field area for 20 min.

For statistical analysis, repeated measures analysis of variance (ANOVA) with the intrasubject factor of time (1–20 min) and the intersubject factor of genotype (−/−, +/−, and +/+) was applied.

2.3.2. Startle response and prepulse inhibition (PPI)

Each mouse was enclosed in a transparent acrylic box (7 cm × 7 cm × 10 cm). Startle response was detected as vibration of the box, using an accelerometer (GH-313A, Keyence, Osaka, Japan). The acoustic startle pulse of broadband burst (115 dB, 50 ms) and tone prepulse (85 dB, 30 ms) were presented via a speaker located in front of the box. Light prepulse (30 ms) was